NAVAL POSTGRADUATE SCHOOL

MONTEREY, CALIFORNIA

THESIS

EXTRACTING MATERIAL CONSTITUTIVE PARAMETERS FROM SCATTERING PARAMETERS

by

Bo-Kai Feng

September 2006

Thesis Advisor: David C. Jenn
Second Reader: Michael A. Morgan

Approved for public release, distribution is unlimited

THIS PAGE INTENTIONALLY LEFT BLANK

REPORT DOCUMENTATION PAGE		*Form Approved OMB No. 0704-0188*

1. AGENCY USE ONLY *(Leave blank)*	2. REPORT DATE September 2006	3. REPORT TYPE AND DATES COVERED Master's Thesis
4. TITLE AND SUBTITLE: Extracting Material Constitutive Parameters from Scattering Parameters		5. FUNDING NUMBERS
6. AUTHOR(S) Bo-Kai Feng		

7. PERFORMING ORGANIZATION NAME(S) AND ADDRESS(ES)
    Naval Postgraduate School
    Monterey, CA   93943-5000
		8. PERFORMING ORGANIZATION REPORT NUMBER

9. SPONSORING /MONITORING AGENCY NAME(S) AND ADDRESS(ES)
    N/A
		10. SPONSORING/MONITORING
		    AGENCY REPORT NUMBER

11. SUPPLEMENTARY NOTES   The views expressed in this thesis are those of the author and do not reflect the official policy or position of the Department of Defense or the U.S. Government.

12a. DISTRIBUTION / AVAILABILITY STATEMENT Approved for public release, distribution is unlimited	12b. DISTRIBUTION CODE

13. ABSTRACT (maximum 200 words)

      In the frequency domain all materials can be described electrically by their complex permittivity (ε) and permeability (μ). These constitutive parameters determine the response of the material to electromagnetic (EM) radiation. The precise knowledge of complex permittivity and permeability is required not only for scientific but also for industrial applications. Due to the uncertainties in manufacturing processes, often the only way to find a material's parameters is to measure them.

      The concept of metamaterials, exhibiting negative permittivity and permeability, is attracting a lot of attention. Such materials are also termed left-handed materials (LHMs).

      This thesis examines several methods to determine the effective permittivity and permeability of both normal materials and metamaterials. CST Microwave Studio is used to model the materials in both free space and rectangular waveguide environments to calculate the S-parameters (S_{11} and S_{21}) from which the constitutive parameters can be extracted.

14. SUBJECT TERMS Complex Permittivity and Permeability, Negative Index, Metamaterials, Constitutive Parameters, S-parameters	15. NUMBER OF PAGES 81
	16. PRICE CODE

17. SECURITY CLASSIFICATION OF REPORT Unclassified	18. SECURITY CLASSIFICATION OF THIS PAGE Unclassified	19. SECURITY CLASSIFICATION OF ABSTRACT Unclassified	20. LIMITATION OF ABSTRACT UL

THIS PAGE INTENTIONALLY LEFT BLANK

EXTRACTING MATERIAL CONSTITUTIVE PARAMETERS FROM SCATTERING PARAMETERS

Bo-Kai Feng
Captain, Taiwan Army
B.S., Chung-Cheng Institute of Technology, 1999

Submitted in partial fulfillment of the
requirements for the degree of

MASTER OF SCIENCE IN SYSTEMS ENGINEERING

from the

NAVAL POSTGRADUATE SCHOOL
September 2006

Author: Bo-Kai Feng

Approved by: David C. Jenn
                        Thesis Advisor

                        Michael A. Morgan
                        Second Reader/Co-Advisor

                        Dan C. Boger
                        Chairman, Department of Information Sciences

THIS PAGE INTENTIONALLY LEFT BLANK

ABSTRACT

In the frequency domain all materials can be described electrically by their complex permittivity (ε) and permeability (μ). These constitutive parameters determine the response of the material to electromagnetic (EM) radiation. The precise knowledge of complex permittivity and permeability is required not only for scientific but also for industrial applications. Due to the uncertainties in manufacturing processes, often the only way to find a material's parameters is to measure them.

The concept of metamaterials, exhibiting negative permittivity and permeability, is attracting a lot of attention. Such materials are also termed left-handed materials (LHMs).

This thesis examines several methods to determine the effective permittivity and permeability of both normal materials and metamaterials. CST Microwave Studio is used to model the materials in both free space and rectangular waveguide environments to calculate the S-parameters (S_{11} and S_{21}) from which the constitutive parameters can be extracted.

THIS PAGE INTENTIONALLY LEFT BLANK

TABLE OF CONTENTS

LIST OF FIGURES

x

THIS PAGE INTENTIONALLY LEFT BLANK

LIST OF TABLES

THIS PAGE INTENTIONALLY LEFT BLANK

ACKNOWLEDGMENTS

THIS PAGE INTENTIONALLY LEFT BLANK

I.   INTRODUCTION

A.   BACKGROUND

In the frequency domain all materials can be described electrically by their complex permittivity (ε) and permeability (μ) which determine their response to electromagnetic (EM) radiation. The precise knowledge of these constitutive parameters is required not only for scientific but also for industrial applications. Due to the uncertainties in manufacturing processes, often the only way to find a material's parameters is to measure them.

In theory, from reflection and transmission measurements, the complex μ and ε can be extracted. However, there are several practical problems that arise, including ambiguities at thicknesses that are multiples of $\lambda/4$. There are even more extraction difficulties when the material under test is a metamaterial, which has complicated frequency dependent material properties.

The transmission and reflection measurements can be done in free space with a large sample of material if care is taken. However, using large samples is undesirable when many different material parameters are being investigated. It is more efficient to take the measurements in a waveguide using small samples. This is referred to as a waveguide simulator, and it has been used for decades in the design of phased array elements [1].

For metamaterials, a retrieval method based on simulation is very attractive. The parameters of the physical materials used to construct the metamaterials are known (e.g., the dielectric substrates and conductors). But the effective parameters are what is needed for designing devices with metamaterials. The effective parameters are the average or macroscopic values that would be presented to an incident field. If the effective values can be found from simulation, it is much more efficient than building samples for testing.

A method that uses reflection measurement has been described by McGinnis [2]. For most cases this general method should work equally as well as the methods shown by Sun [3] and by McGinnis [4]. The latter method is more appropriate if the material has very

high permittivity, permeability or attenuation, or the measurement varies from sample to sample. A newer method [5] using the same concept as [4] but with slightly different formulas, was used in this thesis.

Metamaterials have complex permittivity and permeability that are both negative (double negative, DNG) over some frequency band resulting in a negative index of refraction. This unusual property of metamaterials causes electromagnetic waves to be refracted at a negative angle relative to conventional materials. Various methods to retrieve their constitutive parameters using complex valued reflection (S_{11}) and transmission (S_{21}) coefficients have been developed. One of them is to parametrically fit the S-parameter measurement data to known permittivity (e.g., a Drude model) and permeability (e.g., a Lorentz model). However, this method makes distinct assumptions about the form of the permittivity and permeability. Therefore, in this thesis, methods that directly retrieve the permittivity and permeability are examined and programmed.

B.   OBJECTIVE

The objective of this thesis is to develop and verify methods to retrieve the constitutive parameters of planar materials in free space and waveguide. A wave matrix formulation [6] and formulas from [4] are developed to calculate the reflection and transmission coefficients for arbitrary thicknesses of materials. Free space and waveguide environments are used to extract the permittivity and permeability from the S-parameters. Numerical simulation software, Microwave Studio (MWS) by CST, is used to model the materials and calculate the S-parameters for comparison purposes. The extraction calculation is done in a MATLAB program. To validate the program, many test cases are presented and simulation results are compared to published data.

C.   ORGANIZATION OF THESIS

In Chapter II, metamaterials and their unusual characteristics are discussed. The potential application of metamaterials in waveguide and other applications are presented.

In Chapter III, the free space environment retrieval method is proposed and discussed. The simulation set up using MWS for the free space environment is presented. The results extracted from the S-parameters are compared with published data.

In Chapter IV, the waveguide environment simulation set up and retrieval methods are presented. The extracted permittivity and permeability are described and compared.

Finally in Chapter V, the results, conclusions and suggestions for future studies are discussed.

THIS PAGE INTENTIONALLY LEFT BLANK

II. METAMATERIALS

A. INTRODUCTION

Metamaterials, also called left-handed materials (LHMs), are a class of composite materials artificially built to exhibit unusual properties not found in nature. The history of LHMs can be tracked back to Veselago's theoretical hypothesis in 1968 [7], in which he demonstrated that the LHMs would result in unusual optical phenomena when light passed through them. In 2000, the UCSD (University of California, San Diego) group, which was following the work by Pendry *et al.* [8-10], demonstrated the first left-handed material [11, 12]. This LHM made use of an array of conducting, nonmagnetic elements and an array of conducting continuous wires to achieve a negative effective permittivity and negative effective permeability respectively.

B. NEGATIVE PERMITTIVITY AND PERMEABILITY

In general, for a passive medium, assuming a $e^{j\omega t}$ time dependence,

$$\varepsilon = \varepsilon_r \varepsilon_0 = \left(\varepsilon_r{}' - j\varepsilon_r{}'' \right) \varepsilon_0 \tag{2.1}$$

and

$$\mu = \mu_r \mu_0 = \left(\mu_r{}' - j\mu_r{}'' \right) \mu_0 \tag{2.2}$$

where $\varepsilon_0 = 8.85 \times 10^{-12}\,\text{F/m}$ and $\mu_0 = 4\pi \times 10^{-7}\,\text{H/m}$. For most materials μ and ε are scalars, however, for anisotropic materials, matrices must be used:

$$\bar{D} = \left[\varepsilon \right] \bar{E} \tag{2.3}$$

and

$$\bar{B} = \left[\mu \right] \bar{H} \tag{2.4}$$

where, for example

$$\left[\varepsilon \right] = \varepsilon_0 \begin{pmatrix} \varepsilon_{xx} & \varepsilon_{xy} & \varepsilon_{xz} \\ \varepsilon_{yx} & \varepsilon_{yy} & \varepsilon_{yz} \\ \varepsilon_{zx} & \varepsilon_{zy} & \varepsilon_{zz} \end{pmatrix} \tag{2.5}$$

The elements ε_{ij} ($i, j = x, y$ or z) are the complex relative values that completely describe the permittivity of the material. A similar matrix can be defined for the permeability:

$$[\mu] = \mu_0 \begin{pmatrix} \mu_{xx} & \mu_{xy} & \mu_{xz} \\ \mu_{yx} & \mu_{yy} & \mu_{yz} \\ \mu_{zx} & \mu_{zy} & \mu_{zz} \end{pmatrix} \tag{2.6}$$

Metamaterials are artificial materials that are designed to have unique electromagnetic properties such as a negative index of refraction. For a DNG metamaterial, one should write the permittivity and permeability as [13]:

$$\sqrt{\varepsilon_r} = \sqrt{-|\varepsilon_r|} = j\sqrt{|\varepsilon_r|} \tag{2.7}$$

and

$$\sqrt{\mu_r} = \sqrt{-|\mu_r|} = j\sqrt{|\mu_r|} \tag{2.8}$$

The wavenumber and the wave impedance can be described as follows:

$$k = \omega\sqrt{\varepsilon_0\varepsilon_r}\sqrt{\mu_0\mu_r} = -\omega\sqrt{|\varepsilon_0\varepsilon_r|}\sqrt{|\mu_0\mu_r|} \tag{2.9}$$

and

$$\eta = \eta_0 \frac{\sqrt{\mu_r}}{\sqrt{\varepsilon_r}} = \eta_0 \frac{\sqrt{|\mu_r|}}{\sqrt{|\varepsilon_r|}} \tag{2.10}$$

The index of refraction for a DNG material can be obtained from the formula:

$$n = \sqrt{\varepsilon_r}\sqrt{\mu_r} = -\sqrt{|\varepsilon_r||\mu_r|} \tag{2.11}$$

The different combinations of real permeability and permittivity with various signs are listed in Table 1.

n	$\varepsilon_r > 0$	$\varepsilon_r < 0$
$\mu_r > 0$	+	j
$\mu_r < 0$	j	-

Table 1.   Sign of Index of Refraction

For a DNG material the negative sign flips the angle of refraction in Snell's law. For example, a negative angle of refraction equal and opposite to the standard angle of incidence can be clearly observed in Figure 1.
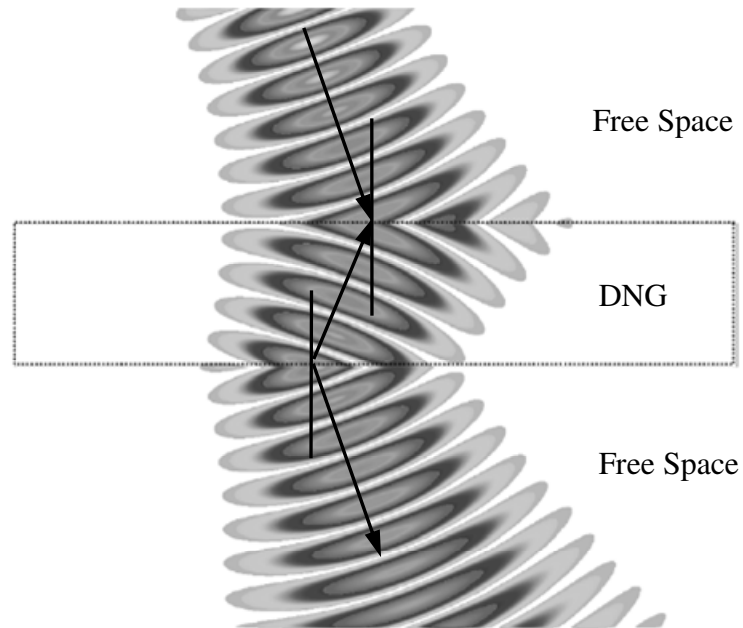
Figure 1.   Electric Field Intensity Distribution for the Wave Interaction with a DNG Metamaterial (After Ref. [13])

As can be seen in Figure 2, on the left, a ray enters a negatively refracting medium and is bent the opposite way relative to the surface normal compared to a conventional right handed material. On the right is the wave vector. Negative refraction requires that the wave vector (direction of phase fronts) and Poynting vector (direction of energy flow) point in opposite directions [13].
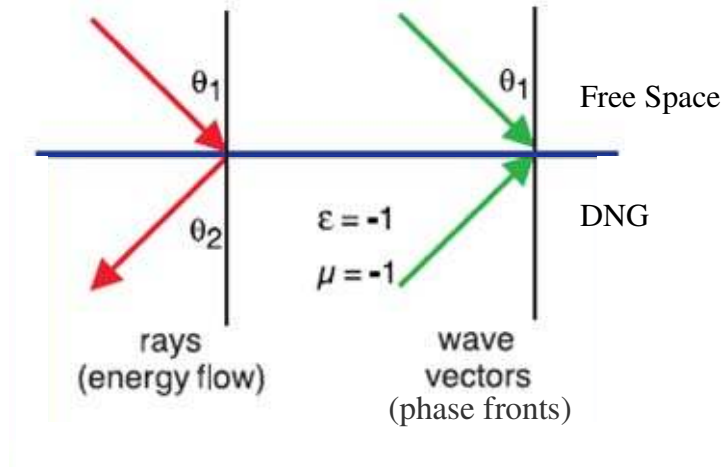
Figure 2.   Depiction of Negative Refraction (After Ref. [13])

The traditional way to build a metamaterial with both negative permeability and permittivity is to use a split ring resonator (SRR) and wire in a unit cell. The metamaterial model built by D. R. Smith is shown in Figure 3. Macroscopically this material behaves as a solid material with an effective permittivity and permeability. This is not surprising if the cell is much smaller than the wavelength of the wave interacting with the material. However it has been found that cell sizes on the order of a fifth of a wavelength are small enough for the material to behave as a homogeneous slab.

Figure 3.   A Negative Index Metamaterial Formed by SRRs and Wires Deposited on Opposite Sides of a Standard Circuit Board. (From Ref. [14])

There are also new concepts for DNG metamaterials. In Chapter III and Chapter IV, these "new" metamaterials were investigated, one of which uses short wire pairs while the other uses H-type pairs as inclusions. The major difference between "traditional" and "new" metamaterials is that "new" metamaterials are relatively easy to fabricate, which make them easier to use and may hasten their development.

C.   APPLICATIONS OF METAMATERIALS

Metamaterials have attracted a lot of attention in recent years. Some of the possible applications of metamaterials are discussed below.

1.   Waveguide Miniaturization

The physical size of a waveguide is an important practical parameter and there is an increased need for miniaturized, compact waveguides. In [15], a method to minimize the waveguide using uniaxial negative permeability metamaterial was proposed. By putting SRRs into the waveguide, a backward passband can occur below the cut-off frequency of the waveguide. In this case, the waveguide supports propagation of backward waves in this passband below the cut-off frequency of the dominant TE mode. The characteristic for this combination presents a chance to construct a smaller waveguide, but still allow the electromagnetic waves to propagate. The schematic of the waveguide loaded with SRRs is as shown in Figure 4.
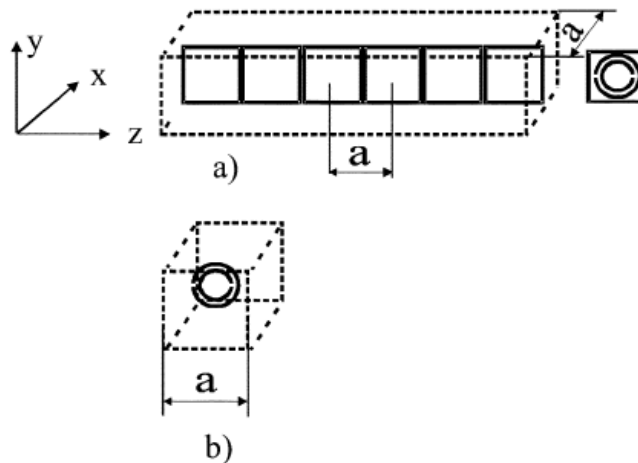
Figure 4.   (a) The Waveguide Filled with the Split Ring Resonators (b) The Unit Cell
(From Ref. [15])

The difference between the waveguides loaded with SRRs with the resonant frequency of SRRs above the cut-off frequency f_c and below f_c ($f_c = 12.5$ GHz for $a = 12$ mm, $f_c = 4.28$ GHz for $a = 35$ mm) is described in Figure 5. Note that when the resonant frequency of SRRs (f_0) is higher than the cut-off frequency of the waveguide, a stop band with negative transversal permeability is observed. On the other hand, when $f_0 < f_c$, a backward passband is observed below the cut-off frequency of the waveguide.
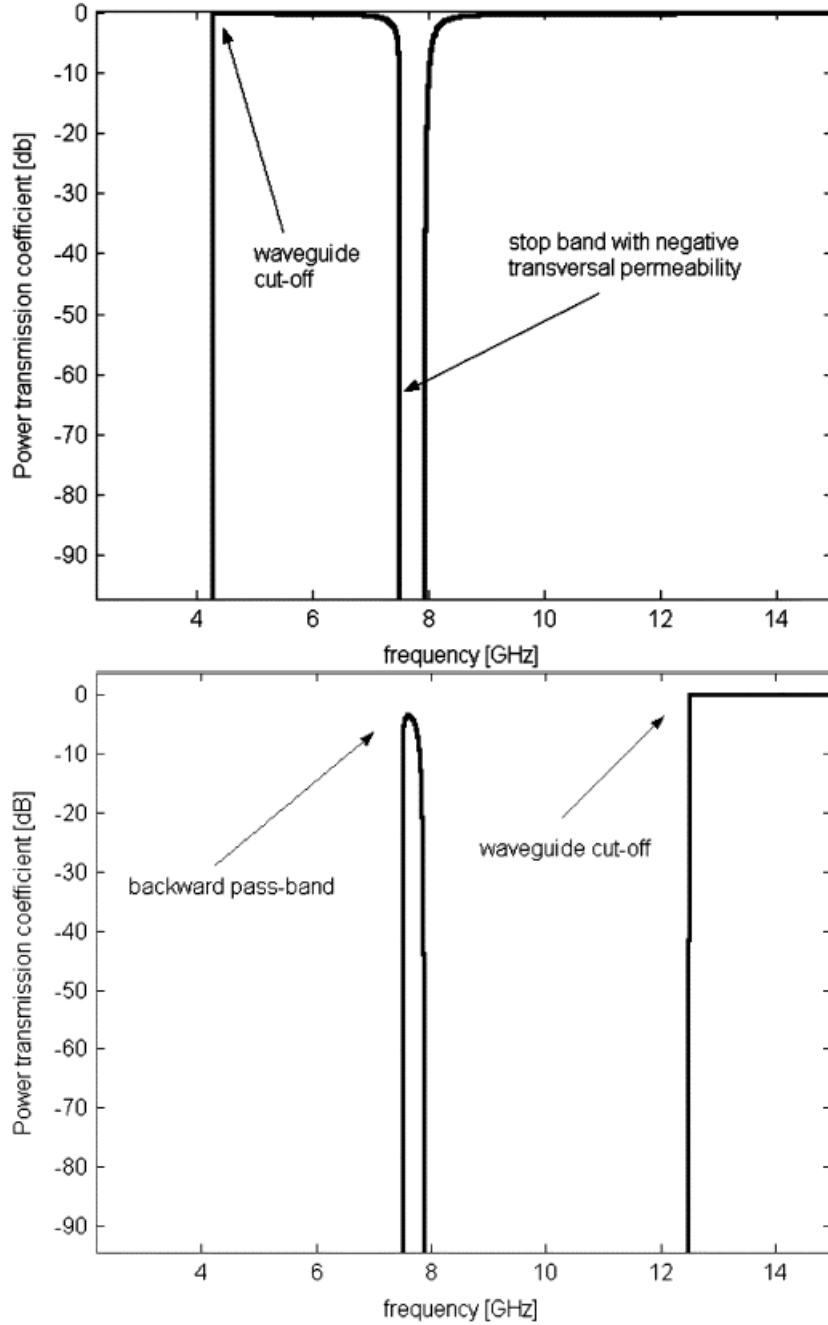
Figure 5.   (a) Calculated Power Transmission Coefficient of the Waveguide (*a*=35 mm)
Filled with Metamaterial Based on Resonant Inclusions
($f_0 = 7.8$ GHz, $f_{mp} = 7.9$ GHz, $\gamma = 1$ MHz , and $f_0 > f_c$). (b) Calculated Power
Transmission Coefficient of the Waveguide (*a*=12 mm) Filled with Metamaterial
Based on Resonant Inclusions ($f_0 = 7.8$ GHz, $f_{mp} = 7.9$ GHz, $\gamma = 1$ MHz , $f_0 < f_c$).
(From Ref. [15])

11

2. Directional Coupler

A DNG-based guiding structure offers a possibility for the "backward" coupling between such guides and the conventional ones. If one of the coupled waveguides carries power in one direction, the second waveguide, placed in its vicinity, will send some of this power in the opposite direction. As the distance between the two guides decreases, the coupling efficiency of the redirected power increases exponentially. A schematic of this kind of coupler is illustrated in Figure 6.
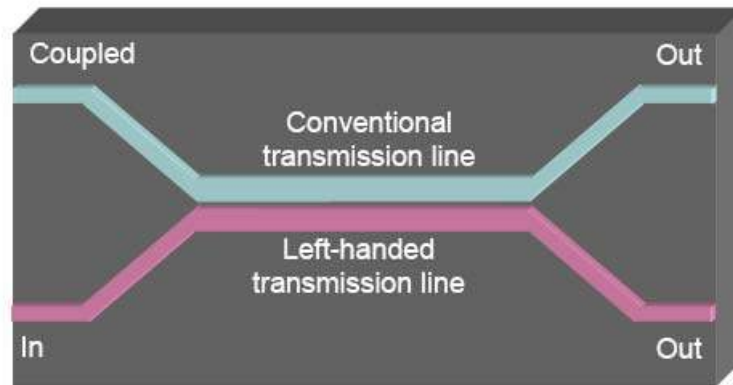
Figure 6.   Schematic of a Metamaterial-based Directional Coupler in Microstrip Implementation (From Ref. [16])

This kind of DNG-based directional coupler has been shown to have improved coupling, a wider range of coupling values than in conventional implementations, and a smaller coupling length.

An experiment has been performed by Eleftheriades [17] where he uses two sets of couplers to compare the coupled power and isolation between Microstrip /Negative-Refractive-Index (MS/NRI) and Microstrip/Microstrip (MS/MS). The results are shown in Figures 7 through 10.
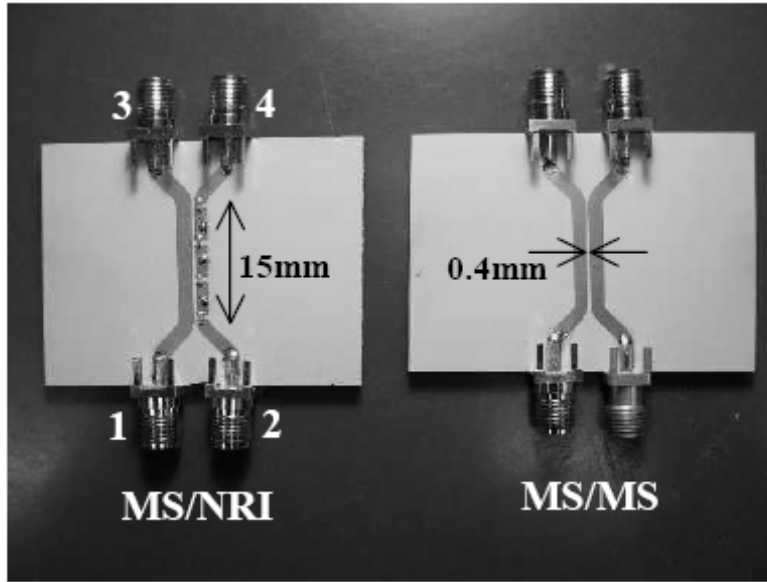
Figure 7.   Microstrip/Negative-Refractive-Index and Microstrip/Microstrip Couplers of Equal Length, Line Spacing, and Propagation Constants (From Ref. [17])
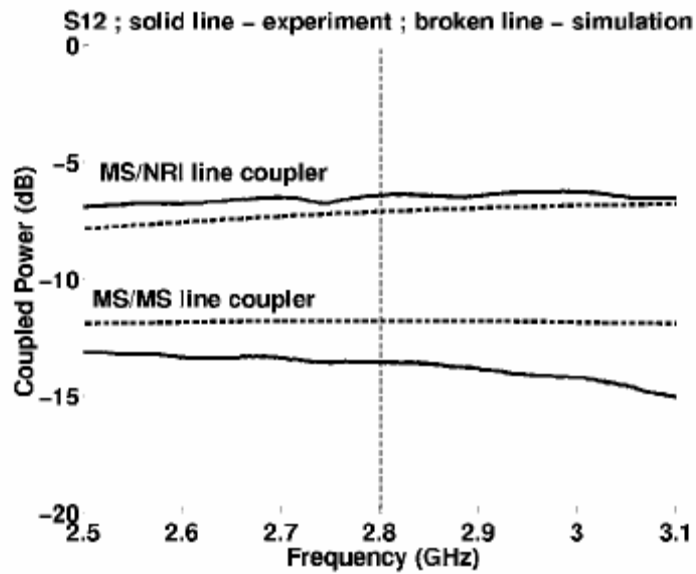
Figure 8.   A Comparison of the Coupled Power Levels for the Microstrip/Negative-Refractive-Index and the Microstrip/Microstrip Couplers (From Ref. [17])
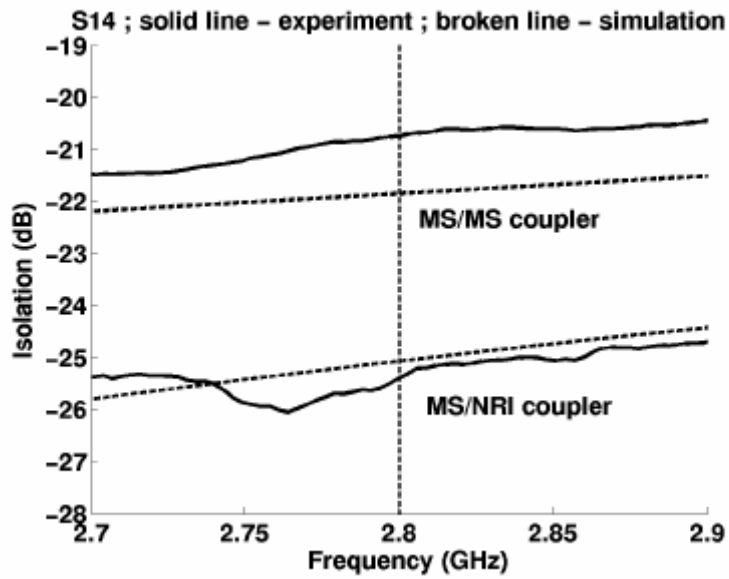
Figure 9.   A Comparison of the Isolation for the Microstrip/Negative-Refractive-Index
and the Microstrip/Microstrip Couplers (From Ref. [17])
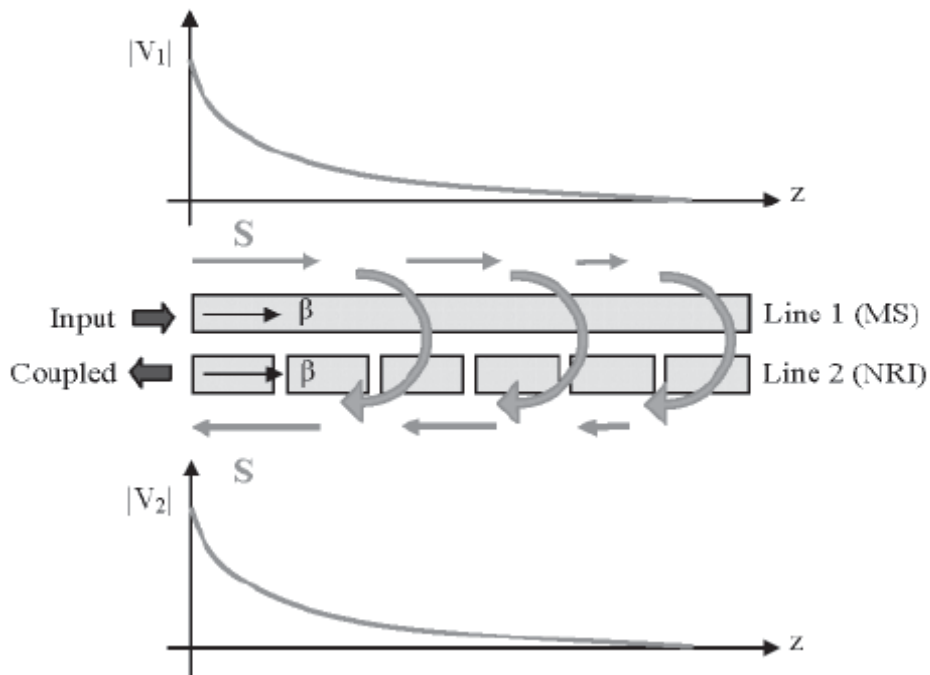
Figure 10.   The Physical Mechanism by which Power Continuously Leaks from the
Microstrip Line to the Negative-Refractive-Index Line (From Ref. [17])

For MS/NRI, the coupled power is 6 dB higher than that in MS/MS (Figure 7) and the isolation for MS/NRI is about 4 dB lower than that in the MS/MS structure (Figure 8). The new MS/NRI coupler exhibits better performance than the traditional MS/MS coupler in terms of higher coupling power, isolation, and lower return loss. The coupling mechanism is depicted in Figure 10.

There are more applications that can exploit the unique characteristics of metamaterials, such as [16]:

1. Wideband directive antennas
2. Perfect lens and superlens
3. Phase compensators and sub-wavelength resonators
4. Guided wave applications
5. Electrically small antennas
6. Filtering and beam shaping

The two examples and the list above include only a few from a wide variety of applications. As more and more people become aware of these new materials and their properties, one can expect to see more applications using metamaterials. In the next chapter the extraction of μ and ε for bulk materials in free space is discussed. The procedure is applied to both conventional materials and metamaterials.

THIS PAGE INTENTIONALLY LEFT BLANK

III. FREE SPACE ENVIRONMENT

A. INTRODUCTION

In this chapter, measurements on materials in the free space environment are used to extract the constitutive parameters from scattering parameters. In order to verify the accuracy of scattering parameters generated from simulation using MWS, the wave matrix approach [18] is used to calculate the reflection and transmission coefficients and compare with those generated from simulation.

B. FORMULATION

The uniform plane waves traveling in the z direction through an infinite slab with relative permittivity ε_r, permeability μ_r, wave impedance η_1 and thickness t is considered. Figure 11 illustrates the simplified model described above.
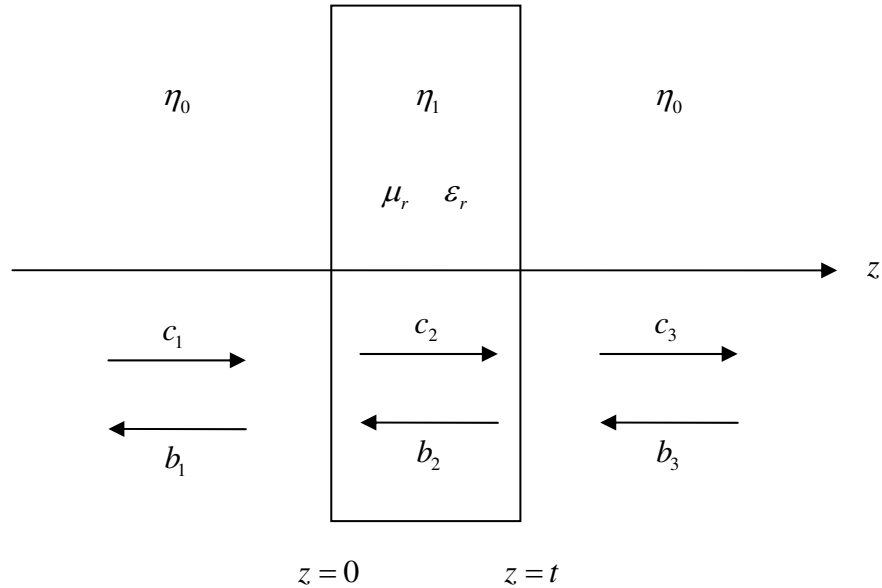
Figure 11.   Schematic of Normal Incidence at an Infinite Slab in Free Space

The general form of the wave matrix formula for a three-layer medium that was used to examine the accuracy of the simulation results is [18]

$$\begin{bmatrix} c_1 \\ b_1 \end{bmatrix} = \prod_{n=1}^{2} \frac{1}{T_n} \begin{pmatrix} e^{j\phi_n} & R_n e^{-j\phi_n} \\ R_n e^{j\phi_n} & e^{-j\phi_n} \end{pmatrix} \begin{bmatrix} c_3 \\ b_3 \end{bmatrix} \equiv \begin{pmatrix} a_{11} & a_{12} \\ a_{21} & a_{22} \end{pmatrix} \begin{bmatrix} c_3 \\ b_3 \end{bmatrix} \tag{3.1}$$

If the thickness of the third layer extends to ∞, then it is possible to state that $b_3 = 0$. The total transmission and reflection coefficients of the slab become

$$T = \frac{c_3}{c_1} = \frac{1}{a_{11}} \tag{3.2}$$

and

$$R = \frac{b_1}{c_1} = \frac{a_{21}}{a_{11}} \tag{3.3}$$

The difference between the calculated and simulated transmission and reflection coefficients for a normal material (both selected μ and ε are positive) are presented in the next section.

The retrieval method used in the first part of this thesis is based on the approach used by Xudong Chen *et al* in [19], where the S-parameters are defined in terms of the reflection and transmission coefficients as

$$S_{11} = R \tag{3.4}$$

and

$$S_{21} = T e^{jk_0 d} \tag{3.5}$$

where k_0 is the wave number in free space and d is the thickness of the material being examined. The impedance Z and the refractive index n are

$$Z = \pm \sqrt{\frac{\left(1 + S_{11}\right)^2 - S_{21}^2}{\left(1 - S_{11}\right)^2 - S_{21}^2}} \tag{3.6}$$

and

$$n = \frac{1}{k_0 d} \left\{ \left[\mathrm{Im}\left[\ln\left(e^{ink_0 d} \right) \right] + 2m\pi \right] - j\left[\mathrm{Re}\left[\ln\left(e^{ink_0 d} \right) \right] \right] \right\} \tag{3.7}$$

where m is an integer related to the branch index of the real part of n and the value of e^{jnk_0d} is obtained from S_{11}, S_{21}, and z from

$$e^{jnk_0d} = \frac{S_{21}}{1 - S_{11}\dfrac{Z-1}{Z+1}} \tag{3.8}$$

As described in [19], Z and n are related so that their relationship can be used to determine the correct sign of Z. Two cases are distinguished in order to correctly find the sign of Z. The first case is for $|\text{Re}(Z)| \geq \delta$, where δ is a positive number and for which $\text{Re}(Z) \geq 0$. In the second case, the sign of Z is chosen so that the corresponding $\text{Im}(n) \geq 0$, or equivalently $|e^{jnk_0d}| \leq 1$. The method to precisely determine the branch of $\text{Re}(n)$ can be found in [19].

C. RETRIEVAL USING NUMERICALLY GENERATED S-PARAMETER

In the first part of this section, it is demonstrated that the simulated data is accurate by comparing it with the data calculated from the wave matrix formula. The effectiveness of the retrieval program is also examined by extracting the constitutive parameters of the model and comparing them with the original values used to compute T and R, and published paper data.

Simulations were done with CST Microwave Studio (Computer Simulation Technology GmbH, Darmstadt, Germany), which uses the finite-integration method in the time domain to determine reflection and/or transmission properties of any given structures.

1. Model 1 - Normal Material

The model used here is a cube with dimension 2.5 mm. The material is given the constitutive parameters $\mu_r = 3$ and $\varepsilon_r = 5$. Boundary conditions are set up to be magnetic $(H_t = 0)$ in the x direction, electric $(E_t = 0)$ in the y direction, and open in the z direction; therefore an infinite slab can be modeled as shown in Figure 12. The plane wave propagates in the negative z direction.
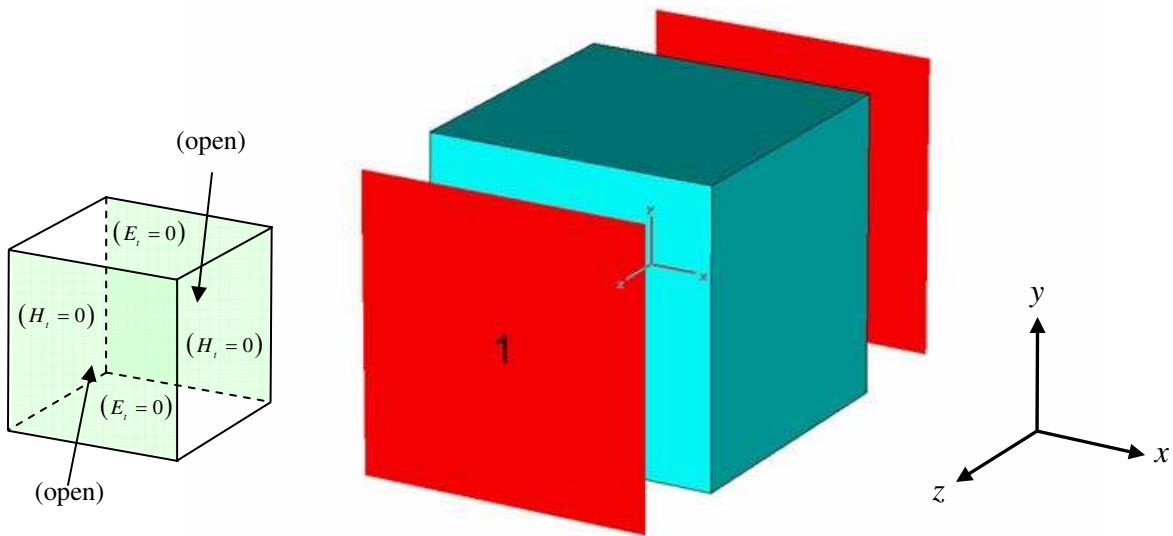
Figure 12.   Normal Material with $\mu_r = 3$ and $\varepsilon_r = 5$, and 2.5 mm side length

The differences between the calculated (using wave matrix formula) and simulated (using MWS) transmission (T) and reflection (R) coefficients are shown in Figures 13 and 14.
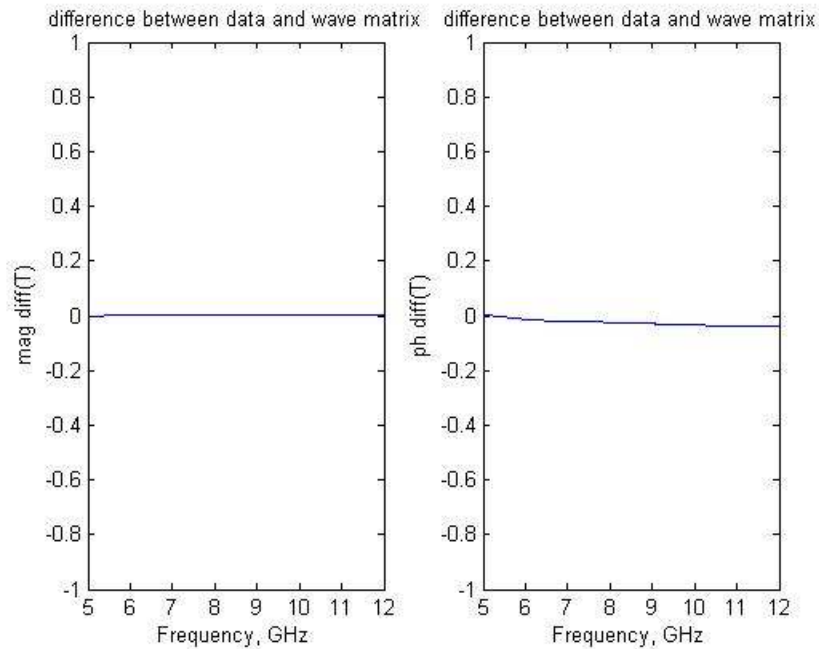
Figure 13.   (a) Magnitude Differences of Transmission Coefficient between the Calculated and Simulated Data (b) Phase Differences (Degrees) of Transmission Coefficient between the Calculated and Simulated Data
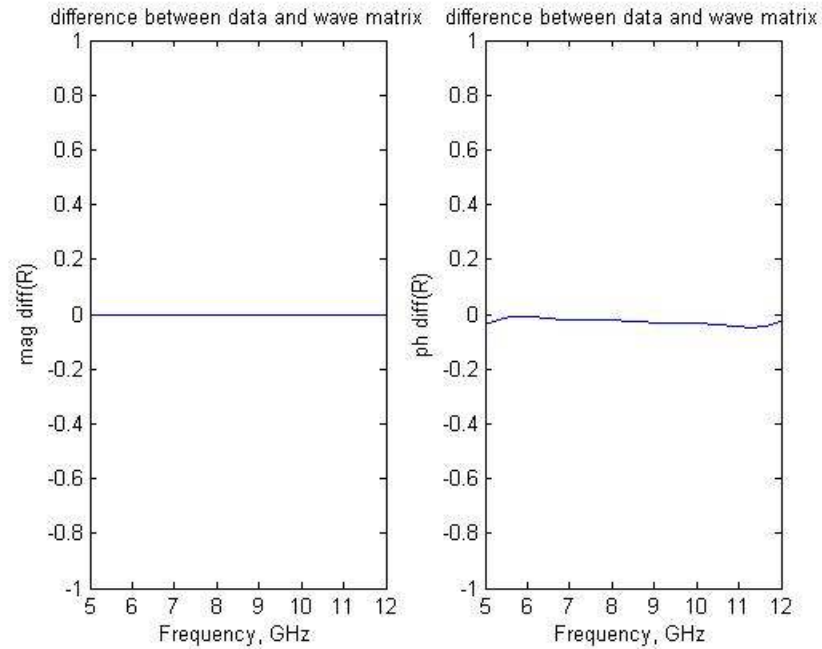
Figure 14.　　(a) Magnitude Differences of Reflection Coefficient between the Calculated and Simulated Data (b) Phase Differences (Degrees) of Reflection Coefficient between the Calculated and Simulated Data

According to Figures 13 and 14, the differences between the calculated and simulated data are almost zero; therefore it can be concluded that the software set up is correct and an infinite panel is simulated. After this simulation accuracy verification, the constitutive parameter retrieval procedure can be conducted based on the same set up.

For the same model and data, an extraction program was used to retrieve the permittivity and permeability from the scattering parameters generated by MWS. The results of the extracted μ_r and ε_r using MATLAB are shown in Figures 15 and 16.
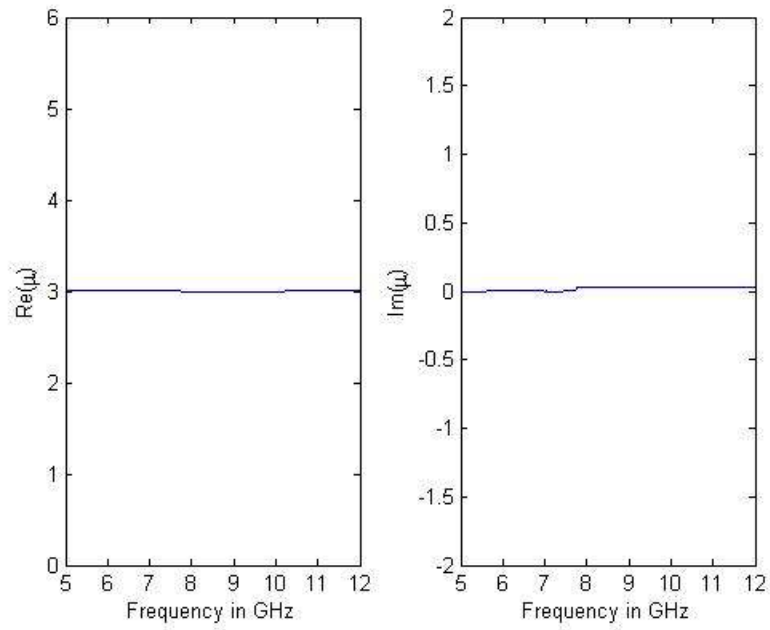
Figure 15.   Extracted Real Part and Imaginary Part of Permeability of Model 1
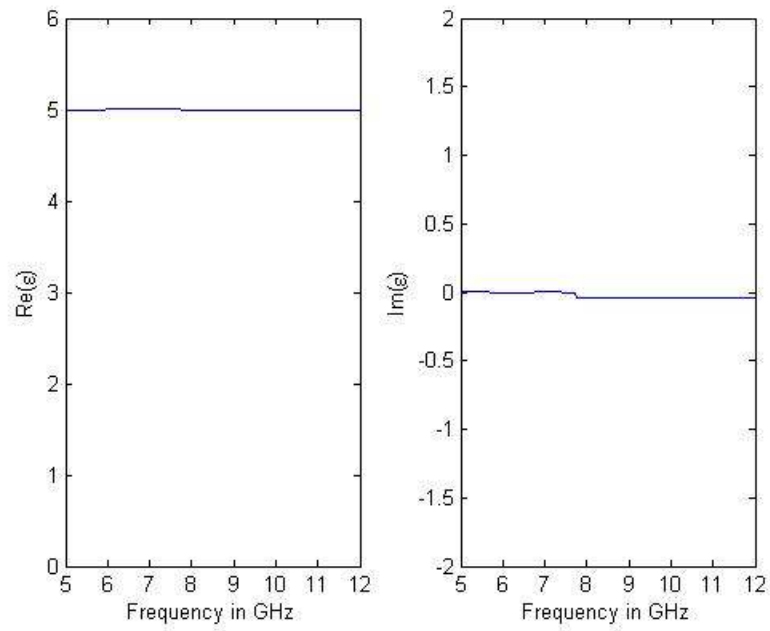
Figure 16.   Extracted Real Part and Imaginary Part of Permittivity of Model 1

The retrieval program correctly extracts the relative permeability (5) and permittivity (3) from the simulation data. Thus, the retrieval program works fine with normal RH material whose constitutive parameters are both positive. Next, the process is extended to LH materials.

2.   Model 2 - "Traditional" Metamaterial

The "traditional" metamaterial model, consists of a split ring resonator (SRR) and wire together to form a material with both negative permittivity and permeability over some frequencies (see Figure 17). The dimensions of this model are the same as described in [20]. The unit cell is cubic, with a cell dimension of $d = 2.5$ mm. A 0.25 mm thick substrate with $\varepsilon = 4.4$, loss tangent of 0.02 is assumed. The copper thickness is 0.017 mm. The width of the wire is 0.14 mm, and it runs the length of the unit cell. The outer ring length of the SRR is 2.2 mm and both rings have a linewidth of 0.2 mm. The gap in each ring is 0.3 mm, and the gap between the inner and outer rings is 0.15 mm. The schematic of this metamaterial slab is shown as Figure 18.
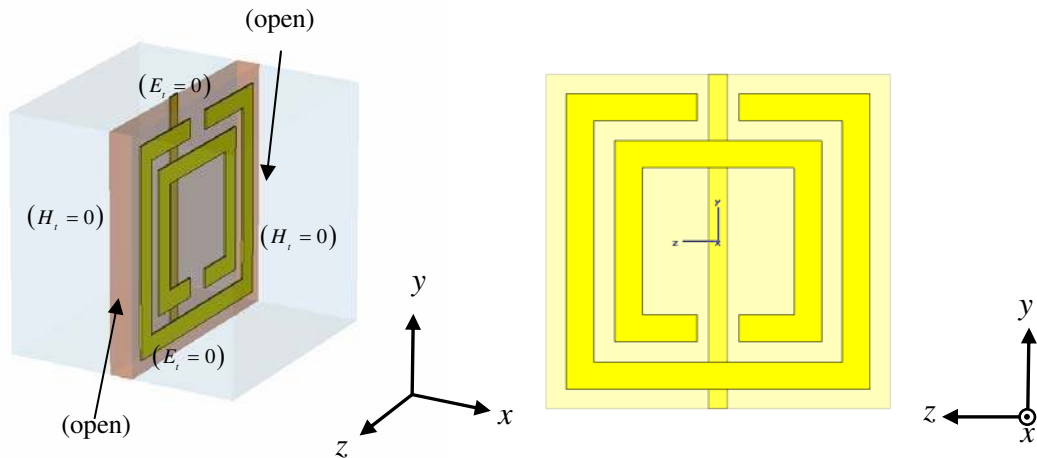
Figure 17.   Model 2 Built in MWS with SRR and Wire. The SRR Provides Negative Permeability While the Wire Provides Negative Permittivity Just Above the Resonant Frequency of the Material

Figure 18.   Schematic of the Metamaterial Slab with Uniform Plane Wave Traveling in the Negative z Direction (Five Layers of Unit Cells in Both x and y Directions are Shown Here)

The same set up as for Model 1 was used, which has the boundary condition $H_t = 0$ in the x direction, $E_t = 0$ in the y direction, and open in the z direction. The boundary condition of this kind not only ensures that the magnetic field goes through SRR but also ensures that the model represents an infinite slab.

The extracted permittivity, permeability, index of refraction, and impedance are shown in Figures 19 through 22.
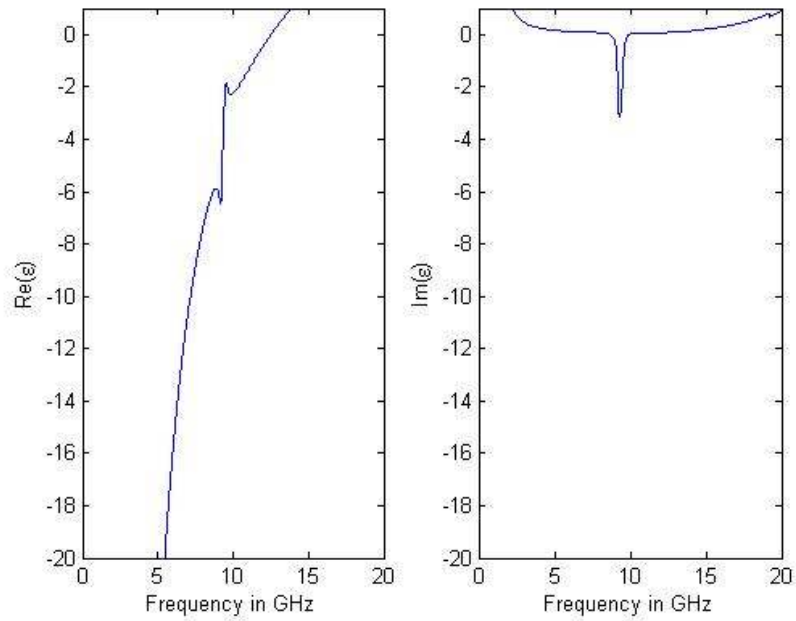
Figure 19.   Extracted Permittivity of Model 2
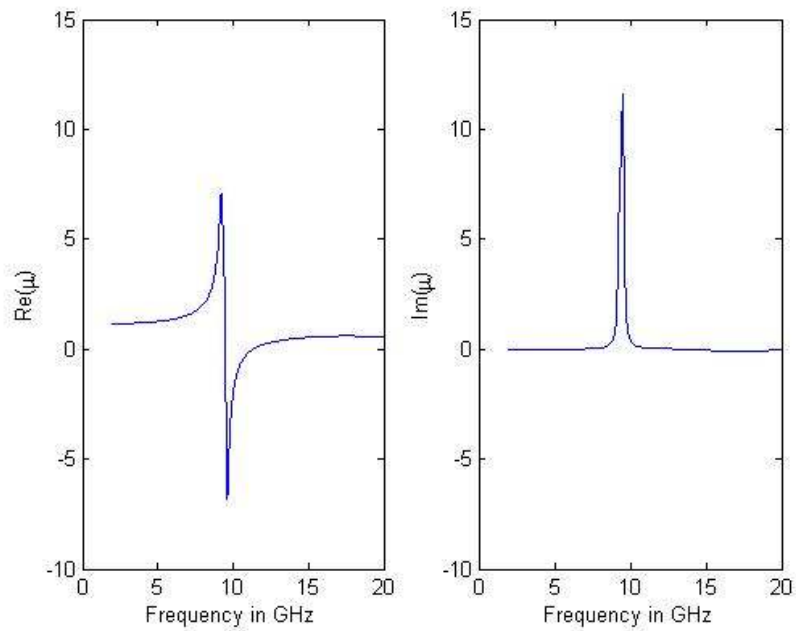
Figure 20.   Extracted Permeability of Model 2
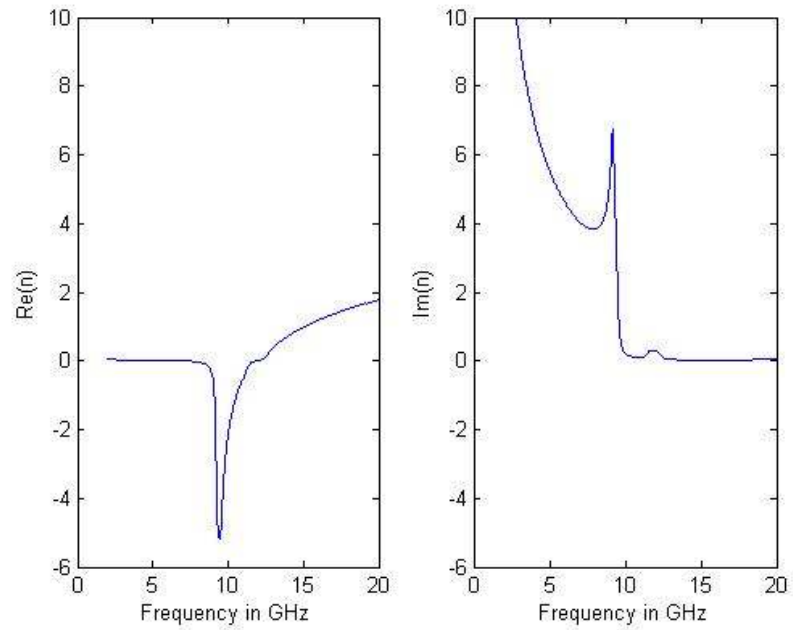
Figure 21.   Index of Refraction of Model 2
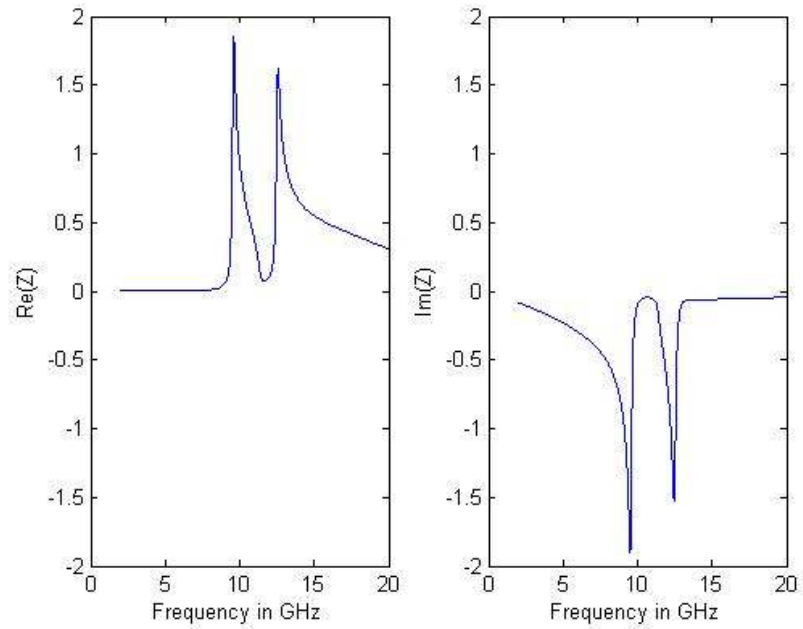
Figure 22.   Impedance of Model 2

The extracted constitutive parameters, index of refraction, and impedance of the material are very close to the published data [20]. However, in the simulation process, it was found that the meshing property is very important in terms of the accuracy of the scattering parameters and the position of the resonant frequency. Because the author does not have the exact meshing parameters which the published paper used, the final results are not identical to the published data, although they are very close.

3. Model 3 - "New" Metamaterial Consisting of Short Wire Pairs

The third model that was used to verify the effectiveness of the program is based on the same structure proposed in [21]. The dielectric layer has a thickness of 254 μm and a relative dielectric constant of 2.53. The copper wire pairs have a thickness 10 μm. The widths of all metal lines are 1 mm. The length of the short wire pairs was 7 mm and the unit cell size was $9.5 \times 7 \times 2.274$ mm^3. In the structure arrangement, the conventional SRR is replaced with a pair of short parallel wires and the continuous wires are preserved (see Figure 23). This "new" structure of metamaterial makes the fabrication procedure much easier. The short wire pairs give the negative permeability and the continuous wires give the negative permittivity over certain frequencies. The schematic of this metamaterial slab is shown as Figure 24.
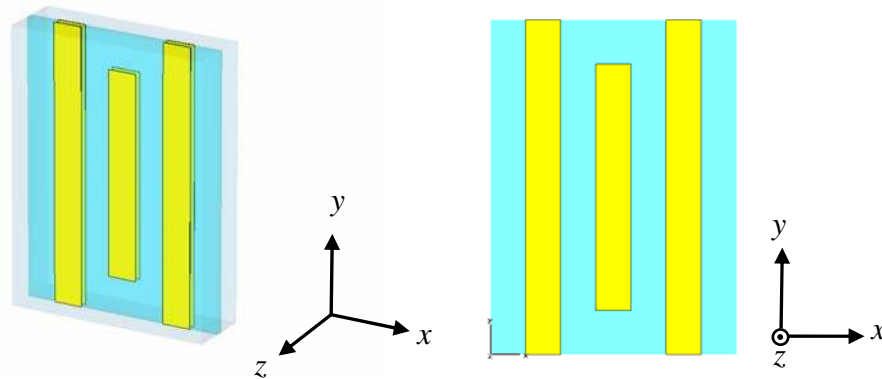
Figure 23.   One Unit Cell of Model 3 Consists of Short-wire Pairs and Continuous Wires
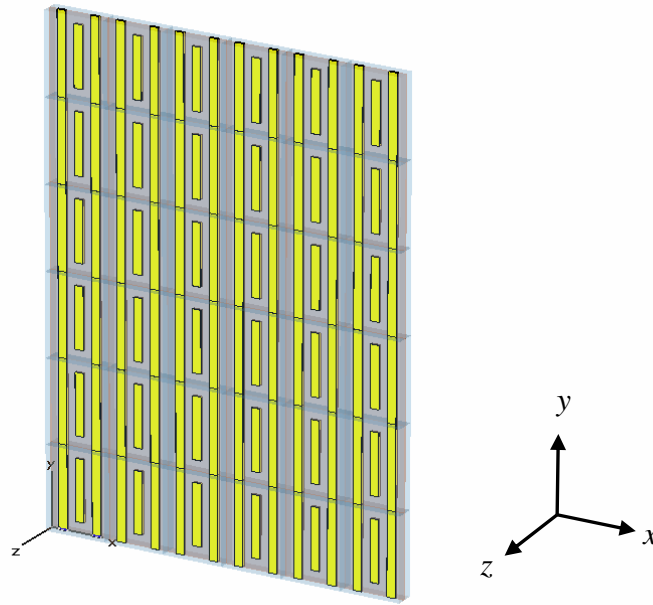
Figure 24.   Schematic of the Metamaterial Slab with Uniform Plane Wave Traveling in the Negative z Direction (Six Layers of Unit Cells in Both x and y Directions are Shown Here)

Figures 25 through 27 show the extracted permeability, permittivity and the refractive index using the simulation data and program. Note that the simulation result is very sensitive to the setting of "mesh cells" in MWS. Different mesh cells can generate slightly different resonant frequencies. One way to avoid this uncertainty is to use the function "adaptive mesh refinement" in MWS. This function is able to calculate the S-parameters with different mesh cells until the difference between the S-parameters is less than the specified value. This method can ensure that the mesh size is small enough to make the results stable.

28

Figure 25.   Extracted Permeability of Model 3
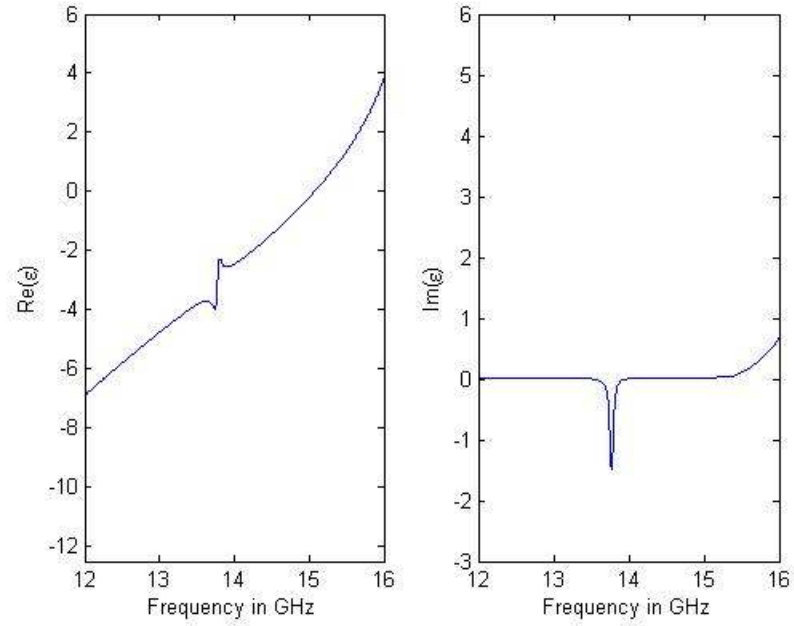
Figure 26.   Extracted Permittivity of Model 3

29
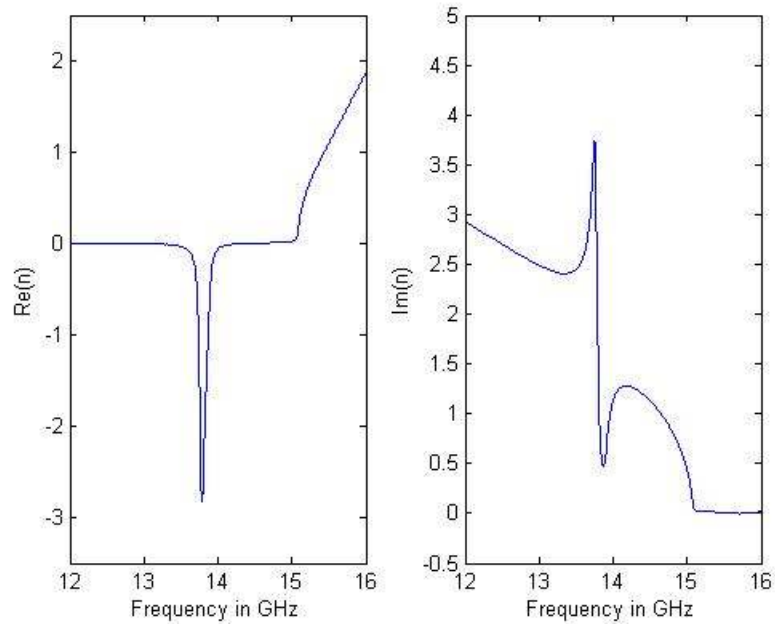
Figure 27.   Refractive Index of Model 3

In comparing the figures with published data in [21], it can be seen that the program discussed in this thesis for the constitutive parameter retrieval from scattering parameters not only can be used for "traditional" metamaterials, but also for the "new" metamaterials.

4.   Model 4 - "New Metamaterial" Consisting of H Type Inclusions

A fourth model considered is also a new metamaterial with H type inclusions. This model is built based on the same dimensions described in [22]. One unit cell of the H type structure is shown in Figure 28. The dielectric-layer thickness is 254 μm and the dielectric constant is 2.53. The copper was formed in the wire pairs patterns have 10 μm thickness. The width of the metal wires was 1 mm. The length and width of the metal bars at each end of the wire pairs were 4 and 0.2 mm, respectively. The length of the short wire pairs was 4 mm, and the unit cell size was $4 \times 8 \times 2.274$ mm^3. The schematic of this metamaterial slab is shown as Figure 29.
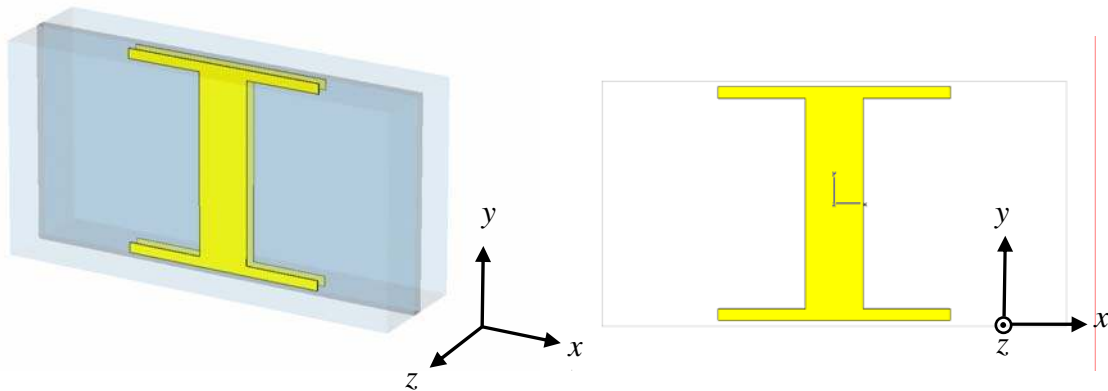
Figure 28.   One Unit Cell of Model 4 Consists of Two H Type Inclusions
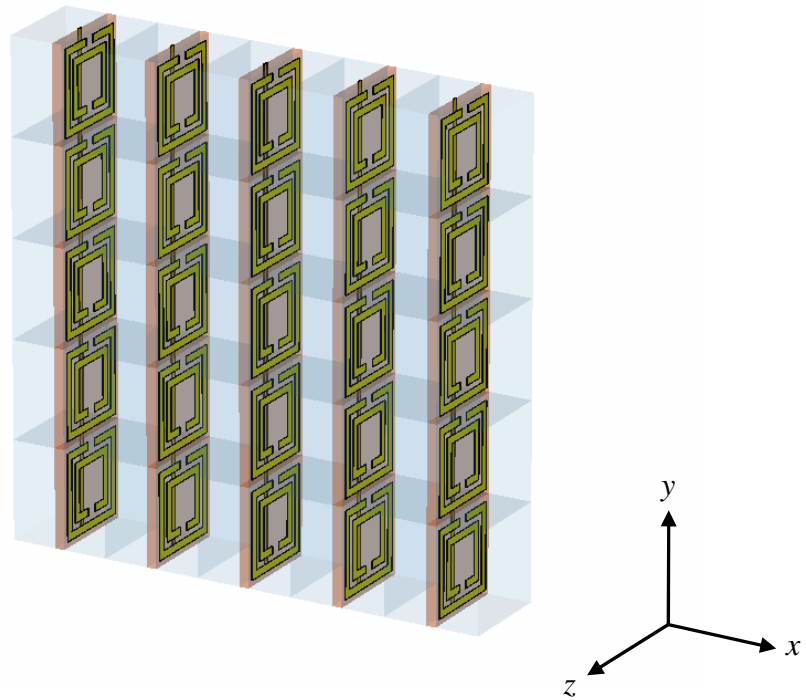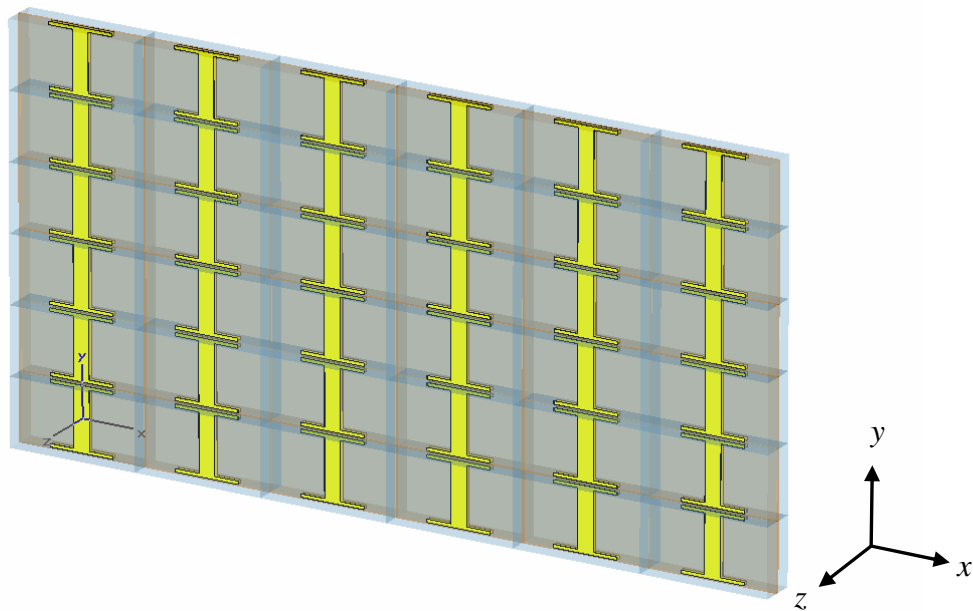

Figure 29.   Schematic of the Metamaterial Slab with Uniform Plane Wave Traveling in the Negative z Direction (Six Layers of Unit Cells in Both x and y Directions are Shown Here)

In order to test the sensitivity of this kind of material relative to the dimension of the inclusions and the number of mesh cells being used for the simulation, the following two scenarios were examined.

a.   *Change the Width of the Bars at Each End of the Wire Pairs*

The width of the metal bars at each end of the wire pairs was slightly changed in order to see the influence on the S-parameters. The width was changed from

0.2 mm to 0.25 mm and the adaptive mesh refinement function was enabled so as to obtain optimal results. The S-parameters for the original 0.2 mm and the modified 0.25 mm structures are presented in Figures 30 and 31.
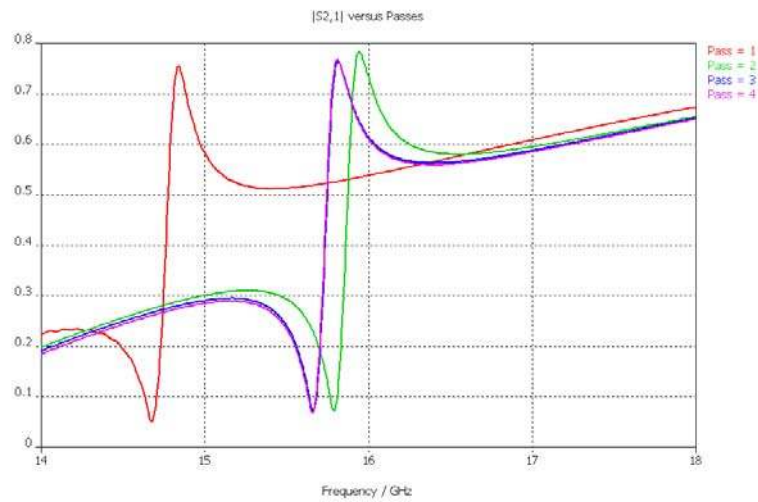
Figure 30.   Magnitude of S_{21} of the Original 0.2 mm Model
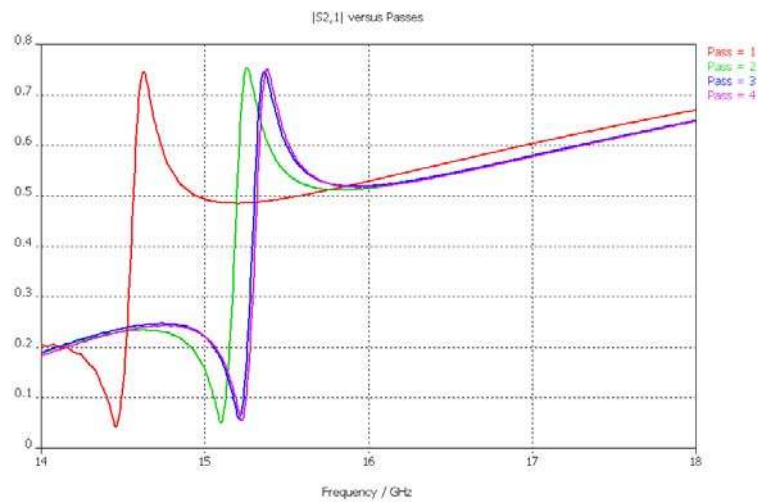
Figure 31.   Magnitude of S_{21} of the Modified 0.25 mm Model

The resonant frequency in Figure 30 with the optimized S_{21} value occurs around 15.65 GHz (purple curve). The optimized resonant frequency in Figure 31 (width

changed by 0.05 mm) shifted to the left to around 15.25 GHz (purple curve). This observation shows that the resonant frequency is very sensitive to the dimension of the inclusions.

b.   Using More Mesh Cells at Simulation Starting Point

For the purpose of understanding the influence of using a different number of mesh cells at the simulation starting point, the meshing parameters in MWS were set up to make the total number of mesh cells higher than the amount used in scenario 1 shown in Figure 30. The simulation result is shown in Figure 32.
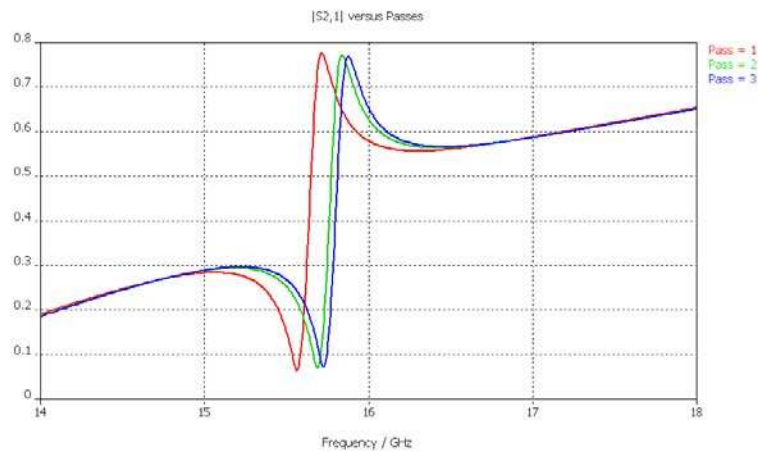
Figure 32.   Magnitude of S_{21} of the Same Model in Figure 29 Except for Using More Mesh Cells as the Simulation Starting Point

It can be clearly seen that using more mesh cells at the starting point (Figure 32) has the resonant frequency of the optimized S_{21} at about 15.75 GHz (blue curve). On the other hand, the one using less mesh cells (Figure 30) has the resonant frequency of the optimized S_{21} at about 15.65 GHz. This is due to the increase in discretization and simulation errors when the mesh size is not optimized and is either too large or too small. As a result, the starting point of the mesh cells number should also be considered in order to get the real optimal value. The other way to make sure the real value is obtained is to compare with measurements.

To compare the retrieved results with the published paper, the closest S-parameter offered in the paper [22], which is shown in Figure 30 pass 2 (green curve), was chosen.

The extracted permeability, permittivity and the index of refraction are provided in Figures 33 through 36 and the results from [22] are in Figure 37 and 38 for comparison purposes.
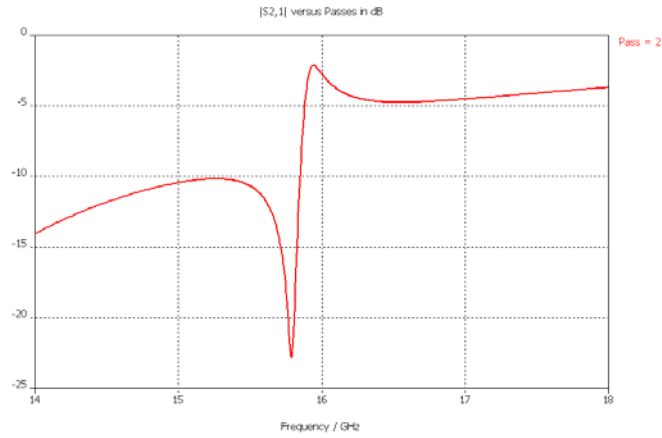
Figure 33.   Simulated S_{21} of the H type Inclusions Metamaterial That is Closest to the Published Data
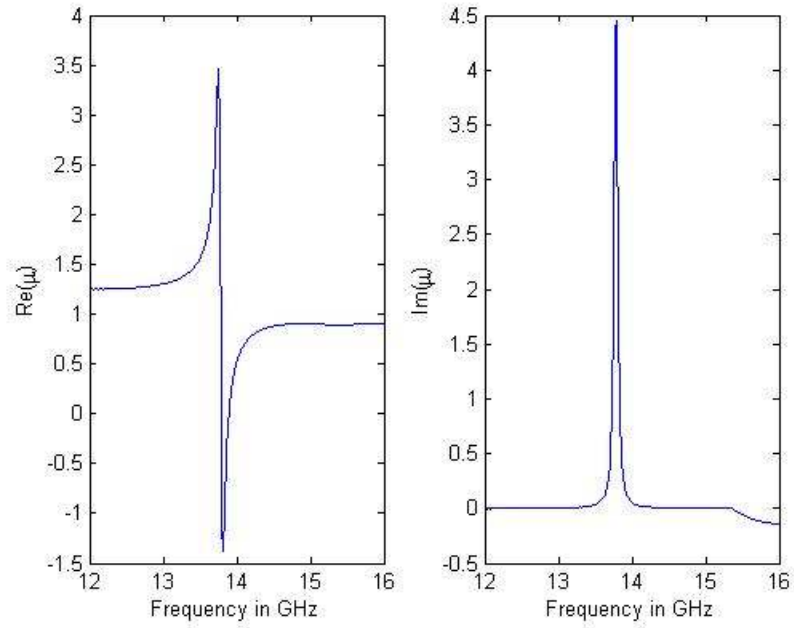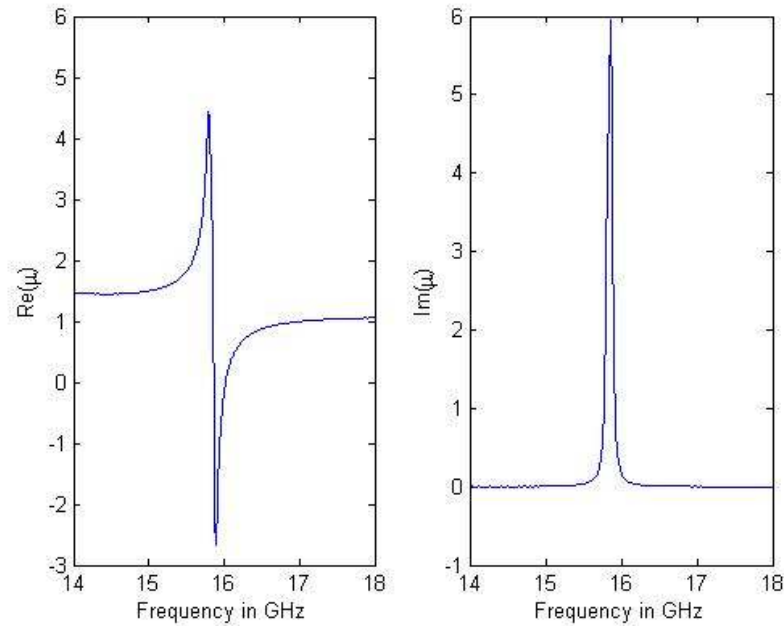

Figure 34.   Extracted Permeability of Model 4
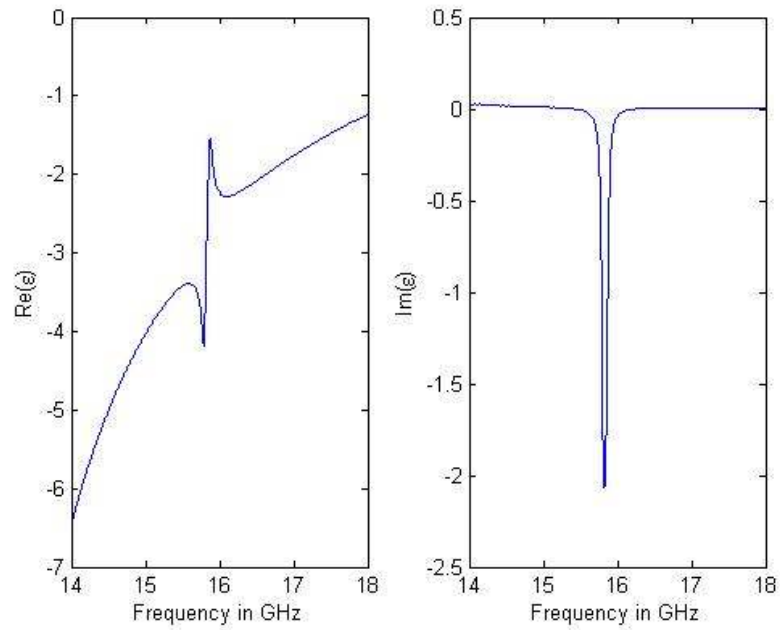
Figure 35.   Extracted Permittivity of Model 4
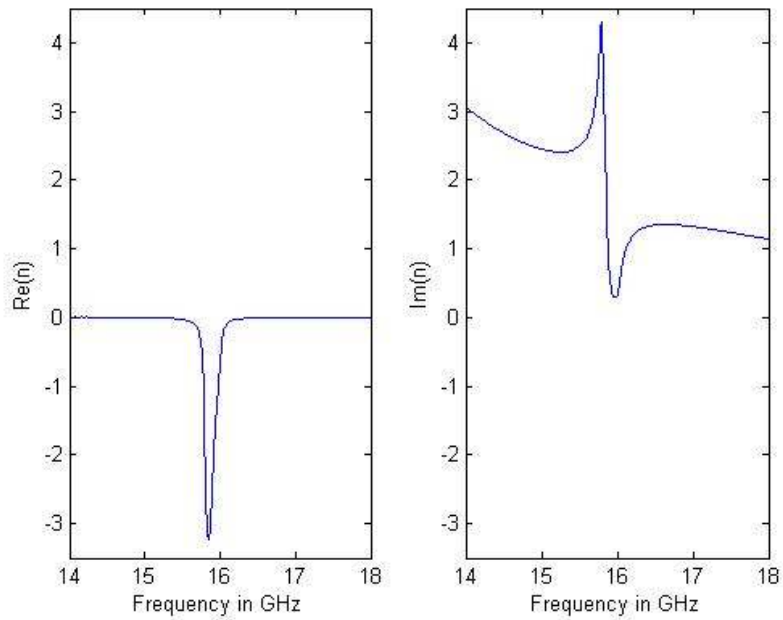
Figure 36.   Refractive Index of Model 4

35
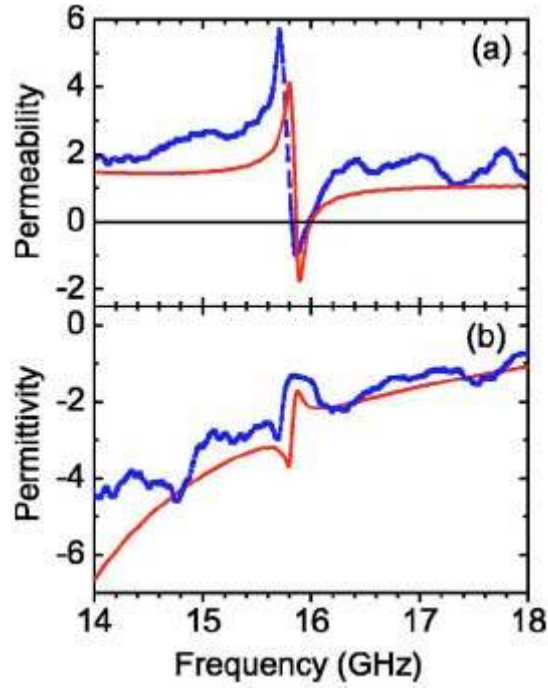
Figure 37.   (a) Extracted Permittivity ε and (b) Permeability μ , Using the Simulated (Red Solid Curves) and Measured (Blue Dotted Curves) Transmission and Reflection Data (From Ref. [22])
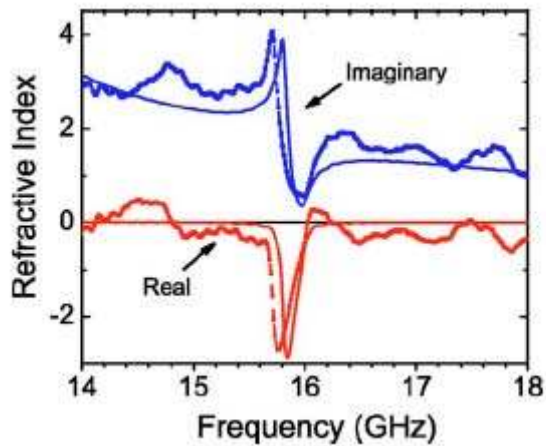
Figure 38.   Extracted Refractive Index n , Using the Simulated (Solid Curves) and Measured (Dotted Curves) Transmission and Reflection Data. The Red and Blue Curves Show the Real Part of n and Imaginary Part of n , Respectively (From Ref. [22])

36

The extracted constitutive parameters and the refractive index are very close to the published data. Again the discrepancy is caused by the simulation set up which is very sensitive to the dimension of inclusions and the number of mesh cells used.

D.   SUMMARY

In this chapter, four models were used to extract the permeability and permittivity from the simulated S-parameters. The formula used was based on the free space environment; therefore boundary conditions had to be defined so that the model could be treated as an infinite slab. Test cases were performed to verify the effectiveness of the simulation set up. It was found that the differences between the simulated and calculated S-parameters were negligible. The resonant frequencies of metamaterial models were very sensitive to both the dimensions and mesh cell number; therefore, it is good to have both simulation and measurement data for comparison purposes. The above models have shown that the extraction program discussed in this thesis can work not only for normal materials but also metamaterials.

THIS PAGE INTENTIONALLY LEFT BLANK

IV.   WAVEGUIDE ENVIRONMENT

A.   INTRODUCTION

In this chapter, a retrieval method for materials in a waveguide environment is used to extract the constitutive parameters of the materials. The purpose of this waveguide method is to demonstrate that the method of images can be applied to structures for permeability and permittivity retrieval. Therefore a small sample of material is enough to perform the extraction or measurement procedure. The results from the free space environment method are also compared to support this hypothesis.

The image principle says that if an object in a metallic waveguide can be imaged properly with respect to the walls, after removing the waveguide walls, the object can be treated as an infinite structure in unbounded space. The equivalent structure is composed of an infinite number of repeated objects in the directions perpendicular to the waveguide walls. An example of the image principle applied to the waveguide model is shown in Figure 39.
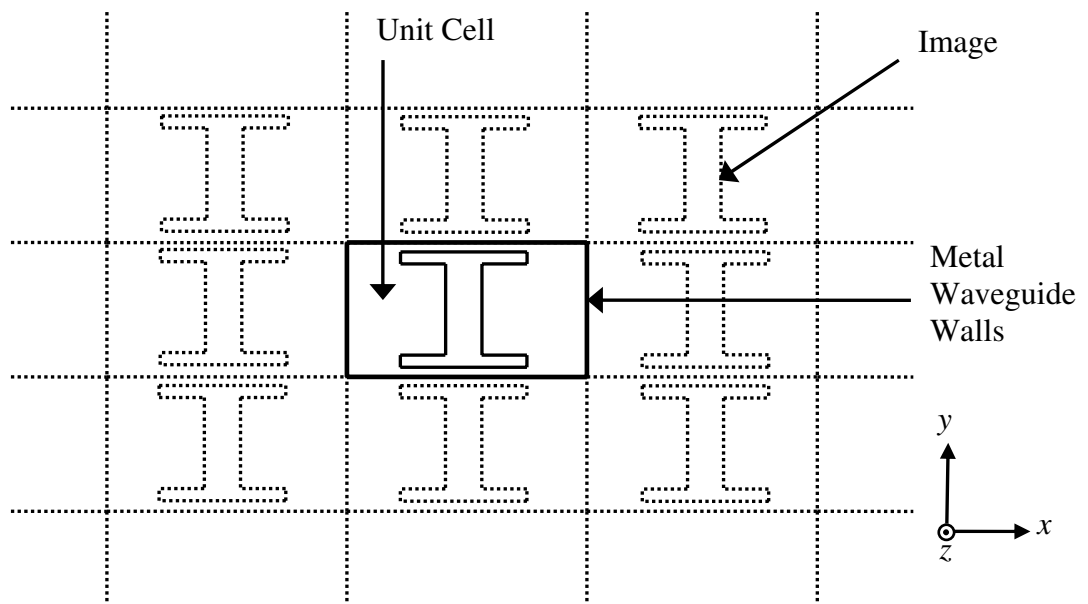
Figure 39.   Image Principle Applied to the Waveguide Retrieval Model

B.   FORMULATION

If the imaging is done properly, waves propagating down the waveguide appear to be incident onto an infinite panel. Generally only the dominant TE_{10} mode is allowed to propagate. It can be decomposed into two plane wave components

$$E_z = E_0 \cos\left(\frac{\pi x}{a}\right) = 2E\left[e^{j\left(\pi\frac{x}{a}-\beta z\right)} + e^{-j\left(\pi\frac{x}{a}+\beta z\right)}\right] \qquad (4.1)$$

and the angles of incidence with respect to the sample face normal are $\pm\tan^{-1}\left[\pi/\beta a\right]$. Only a few angles will be possible given the restrictions on imaging the structure. Note that the electrical size of a must be large to obtain near normal incidence but should be limited to only have TE_{10} mode. More cells must be used, which increases the number of mesh nodes and simulation time.

Consider a material of thickness δ that is placed in a waveguide. The distances from the front face and back face of the material to the two openings of the waveguide are d_1 and d_2. The material is perpendicular to the direction of the propagating electromagnetic waves. It is assumed that only the fundamental waveguide mode TE_{10} can propagate. The geometry for the waveguide retrieval method is shown below in Figure 40. The scattering parameters can be determined by measurement with a physical system, or by simulation with computational electromagnetic (CEM) software.
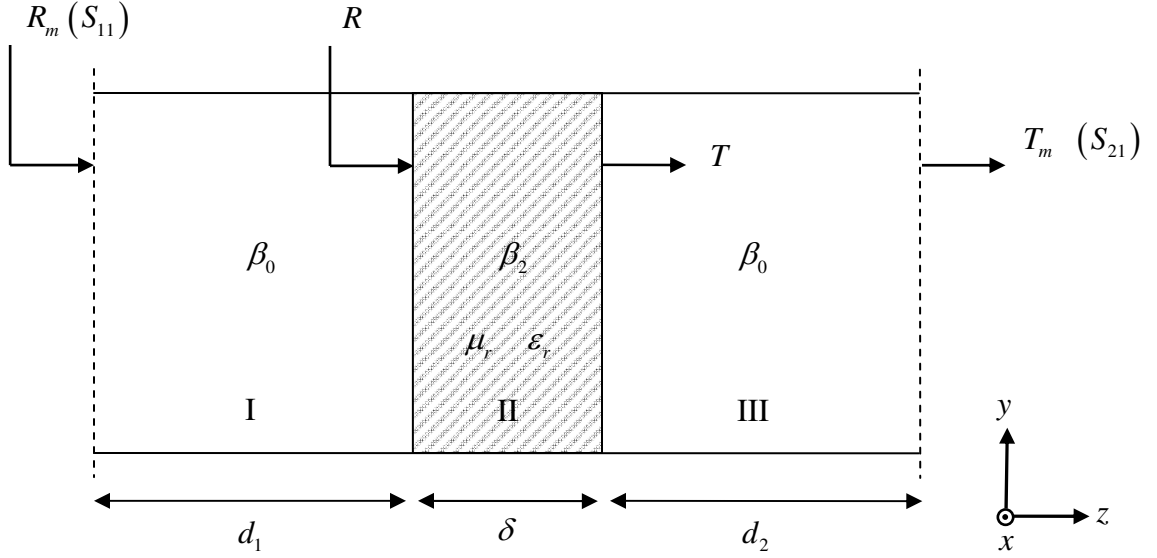
Figure 40.   Schematic of Waveguide S-parameter Retrieval Setup (After Ref. [4])

The formulas used to verify the MWS model set up are from [4]. In the case of a given μ_r and ε_r, the S-parameters $S_{11}(=R_m)$ and $S_{21}(=T_m)$ can be obtained from the equations that follow.

First, the propagation constant in the waveguide filled with free space and the material are defined as β_0 and β_2 respectively,

$$\beta_0^{\ 2} = \left(\frac{\omega}{c}\right)^2 - \left(\frac{\pi}{a}\right)^2 \tag{4.2}$$

and

$$\beta_2^{\ 2} = \mu_r \varepsilon_r \left(\frac{\omega}{c}\right)^2 - \left(\frac{\pi}{a}\right)^2 \tag{4.3}$$

The reflection coefficient and transmission coefficient at the material surfaces can be described as follows:

$$R = R_2 \frac{1 - e^{j2\beta_2\delta}}{R_2^{\ 2} - e^{j2\beta_2\delta}} \tag{4.4}$$

41

and

$$T = e^{-j\beta_2\delta}\left(1 - RR_2\right) \tag{4.5}$$

with

$$R_2 = \frac{\mu_r\beta_0 - \beta_2}{\mu_r\beta_0 + \beta_2} \tag{4.6}$$

For the case where the waveguide is not fully filled, which is the case in Figure 40, the distances between material surfaces and the openings of the waveguide d_1 and d_2 must be included in the formula in order to have the correct phase of the S-parameters. Therefore, the final reflection and transmission coefficients can be described as

$$S_{11} = R_m = Re^{-j2\beta_0 d_1} \tag{4.7}$$

and

$$S_{21} = T_m = Te^{-j\beta_0(d_1+d_2)} \tag{4.8}$$

This formula was compared to the MWS simulated S-parameters to make sure the simulation set up in the waveguide was correct. The comparison is shown in the next section.

The retrieval method used in the second part of this thesis is based on the approach used by Zwick *et al* in [23], where the S-parameters are defined in terms of the reflection and transmission coefficients as

$$S_{11} = \frac{R(1-T^2)}{1-R^2T^2}e^{-j2\gamma_0 d_1} \tag{4.9}$$

$$S_{21} = \frac{T\left(1-R^2\right)}{1-R^2T^2}e^{-j\gamma_0(d_1+d_2)} \tag{4.10}$$

Equations (4.9) and (4.10) can be solved for R:

$$R = \frac{K \pm \sqrt{K^2 - 4S_{11}^{\,2}}}{2S_{11}} \tag{4.11}$$

42

with

$$K = S_{11}^{2} - S_{21}^{2} + 1 \qquad (4.12)$$

and

$$T = \frac{S_{11} + S_{21} - R}{1 - R(S_{11} + S_{21})} \qquad (4.13)$$

In Equation (4.11), the sign of the square root has to be chosen such that $|R| \leq 1$. The parameters γ and γ_0 can be calculated as follows:

$$\gamma = \frac{j2k\pi - \ln(T)}{\delta} \qquad (4.14)$$

and

$$\gamma_0 = j2\pi \sqrt{f^2 \mu_0 \varepsilon_0 - \left(\frac{1}{2a}\right)^2} \qquad (4.15)$$

with k being an integer value, f the frequency, and a the width of the waveguide. The details on how to choose the correct k is described in [23]. Basically, k is first split into a frequency-dependent part $k(f)$ and an offset k_0 as follows:

$$k = k_0 + k(f) \qquad (4.16)$$

where $k(f)$ is simply determined by using the fact that the phase of T has to be monotonically decreasing without large steps. The constant k_0 can be obtained by finding the k_0 for which ε_r and μ_r are almost constant over frequency. The complex permeability and permittivity are finally determined as

$$\mu = \mu_0 \frac{\gamma(1+R)}{\gamma_0(1-R)} \qquad (4.17)$$

and

$$\varepsilon = \frac{\left(\dfrac{1}{2a}\right)^2 - \left(\dfrac{\gamma}{2\pi}\right)^2}{\mu f^2} \qquad (4.18)$$

C. RETRIEVAL USING NUMERICALLY GENERATED S-PARAMETERS

1. Model 5 - Normal Material in Waveguide

Model 5 is a normal (RH) material slab with relative permeability (3) and permittivity (5). The dimension of this slab is $8 \times 4.2 \times 2.274$ mm^3. Boundary conditions are chosen to be electric $(E_t = 0)$ on the top and bottom and side walls. The schematic of this model is shown in Figure 41.
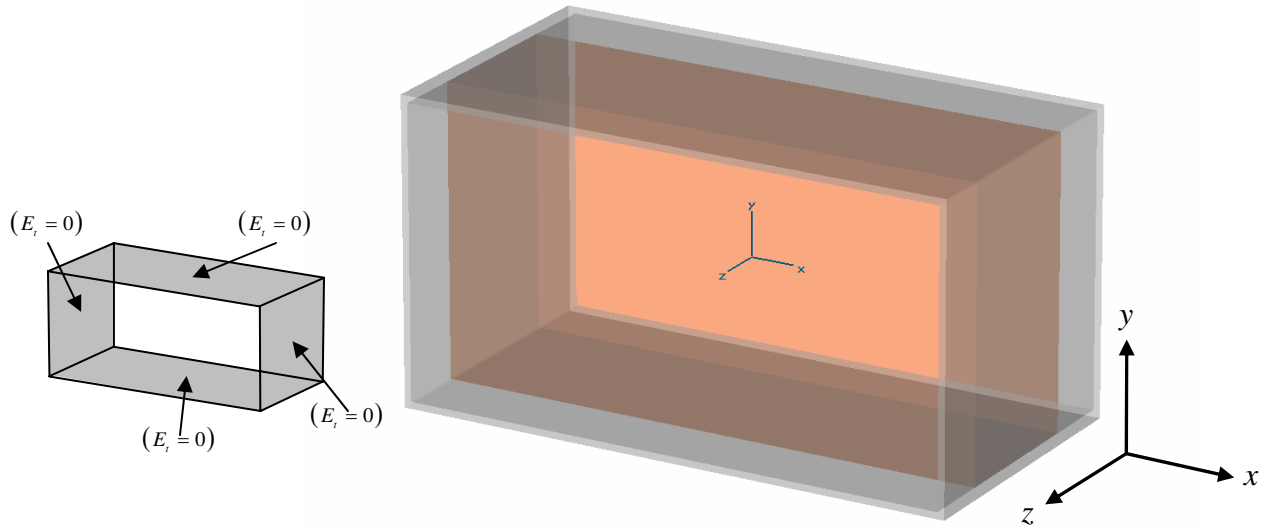
Figure 41.   Normal Slab Material with $\mu_r = 3$ and $\varepsilon_r = 5$ in a Waveguide. The Dimension of the Slab is $8 \times 4.2 \times 2.274$ mm^3.

The operating frequency must be above the cut-off frequency of the waveguide such that the electromagnetic waves can propagate through the waveguide. In the simulation, it is required that only the fundamental TE_{10} mode can propagate. Therefore, not only is it necessary to operate above the cut-off frequency but it is also necessary to prevent higher modes from being generated. Cut-off frequency for the waveguide can be calculated from the formula

$$\left(f_c \right)_{mn} = \frac{1}{2\sqrt{\mu\varepsilon}} \sqrt{\left(\frac{m}{a}\right)^2 + \left(\frac{n}{b}\right)^2} \quad \text{(Hz)} \tag{4.19}$$

For this model, the width of the waveguide is $a = 8$ mm and the height of the waveguide is $b = 4.2$ mm, and $\mu = \mu_0$ and $\varepsilon = \varepsilon_0$ for free space. The operating frequency range for this waveguide can be chosen from Table 2.

$\left(f_c \right)_{mn}$	$m = 1$	$m = 2$	$m = 3$
$n = 0$	18.74 GHz	37.48 GHz	56.22 GHz
$n = 1$	40.32 GHz	51.76 GHz	66.60 GHz
$n = 2$	73.81 GHz	80.64 GHz	90.88 GHz
$n = 3$	108.72 GHz	113.46 GHz	120.96 GHz

Table 2.   Cut-off Frequencies for Waveguide with $a = 8$ mm and $b = 4.2$ mm.

According to Table 2, the operating frequency should be chosen between 18.74 and 37.48 GHz to only allow the TE_{10} mode to propagate.

As described in Section C of Chapter III, the calculated and simulated transmission (T) and reflection (R) coefficients were compared in order to verify the set up in MWS. The formulas used were the ones described in Section B. The compared results are presented in Figure 42 and Figure 43.
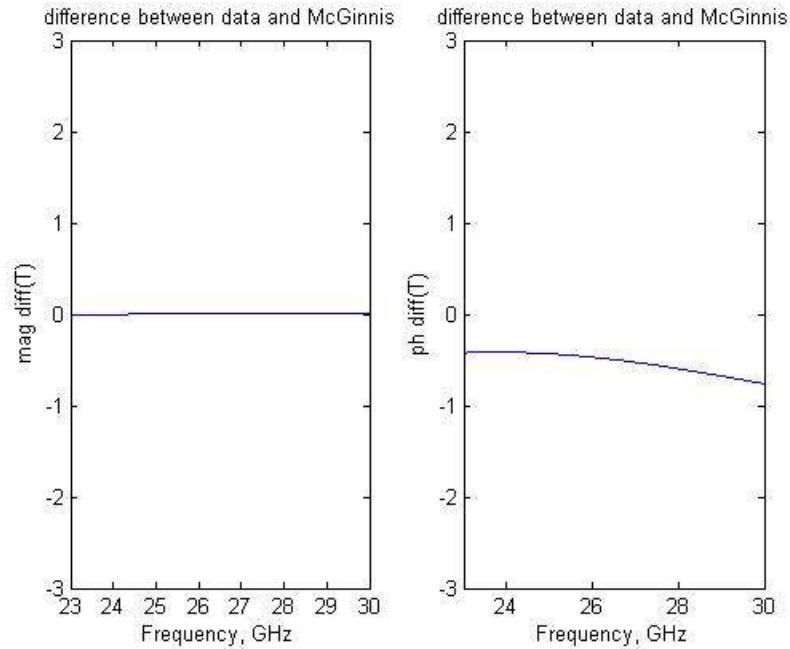
Figure 42.   (a) Magnitude Differences of Transmission Coefficient between the Calculated and Simulated Data (b) Phase Differences (Degrees) of Transmission Coefficient between the Calculated and Simulated Data
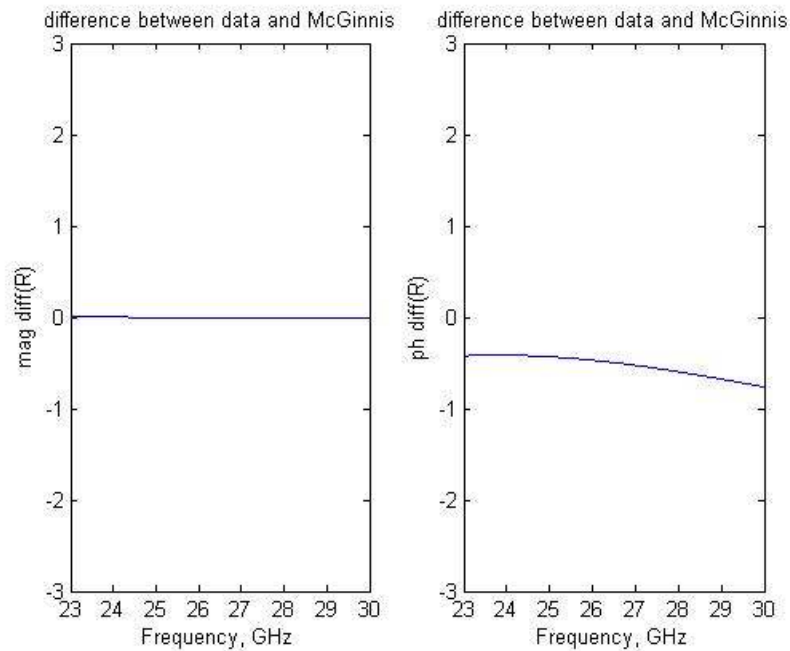
Figure 43.   (a) Magnitude Differences of Reflection Coefficient between the Calculated and Simulated Data (b) Phase Differences (Degrees) of Reflection Coefficient between the Calculated and Simulated Data

According to the Figures 42 and 43, the differences between the calculated and simulated data for the real parts of the transmission and reflection coefficients are almost zero. There is less than a one degree phase difference in both the transmission and reflection coefficients, which is acceptable. Therefore, the simulation set up is considered correct and the results are acceptable.

For the same model and data that was presented above, an extraction program is used to retrieve the permittivity and permeability from the scattering parameters generated from MWS. Figures 44 and 45 show the results for the extracted μ_r and ε_r using MATLAB.
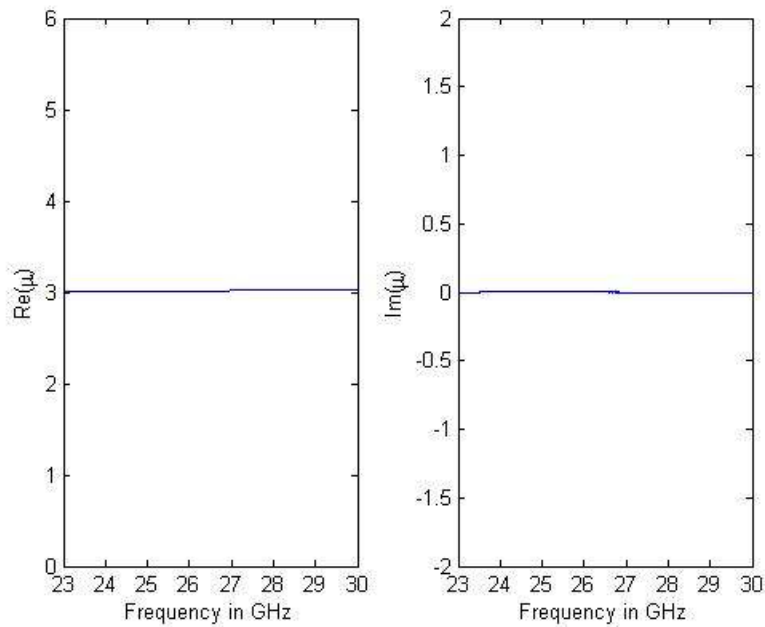
Figure 44.   Extracted Real Part and Imaginary Part of the Permeability of Model 5
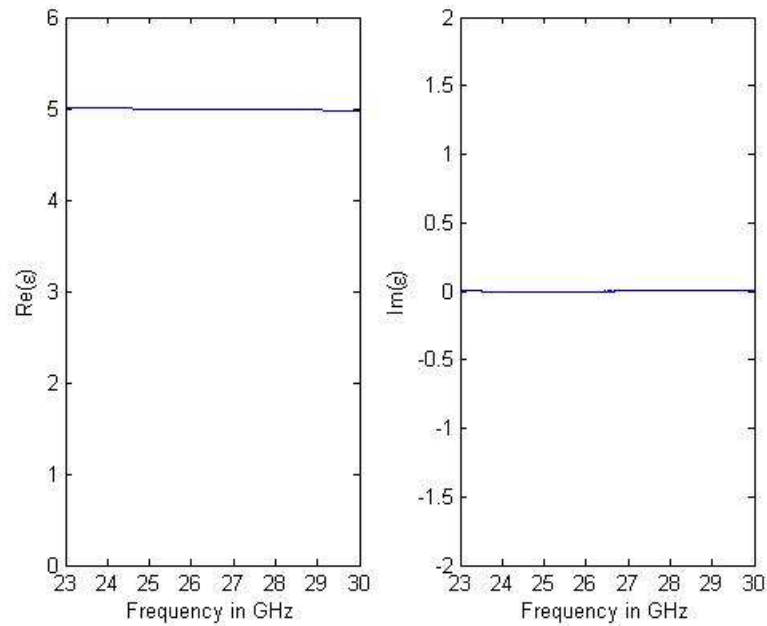
Figure 45.   Extracted Real Part and Imaginary Part of the Permittivity of Model 5

The constitutive parameters were successfully extracted from the simulated S-parameters. Besides, it was found that although there was less than one degree phase difference between the simulated and calculated S-parameters, the differences did not have a big influence on the extracted permeability and permittivity.

2.   Model 6 - "New" Metamaterial---H Type Metamaterial in Waveguide

In order to compare with the results from model 4, which used the free space method to extract the constitutive parameters, the dimensions of the waveguide were chosen so that the waveguide can operate at the same frequency range as in free space (model 4). The related dimensions and cut-off frequencies are listed in Table 3 and Table 4.

$(f_c)_{mn}$	$m=1$	$m=2$	$m=3$
$n=0$	9.37 GHz	18.74 GHz	28.11 GHz
$n=1$	36.91 GHz	40.32 GHz	45.44 GHz
$n=2$	72.01 GHz	73.81 GHz	76.73 GHz
$n=3$	107.5 GHz	108.72 GHz	110.72 GHz

Table 3.   Cut-off Frequencies for Waveguide with $a=16$ mm and $b=4.2$ mm.

$(f_c)_{mn}$	$m=1$	$m=2$	$m=3$
$n=0$	6.25 GHz	12.49 GHz	18.74 GHz
$n=1$	36.24 GHz	37.82 GHz	40.32 GHz
$n=2$	71.67 GHz	72.48 GHz	73.81 GHz
$n=3$	107.28 GHz	107.82 GHz	108.72 GHz

Table 4.   Cut-off Frequencies for Waveguide with $a=24$ mm and $b=4.2$ mm.

According to Tables 2, 3, and 4, the width of the waveguide a can only be chosen to be 16 mm so that the simulation can run in the frequency range of 14 to 18 GHz and only the TE_{10} mode will propagate in the waveguide.

The schematic of the H-type inclusion metamaterial in the waveguide environment is shown in Figure 46. The boundary condition setting is the same as in model 5. The waveguide dimensions are $a=16$ mm and $b=4.2$ mm.

49
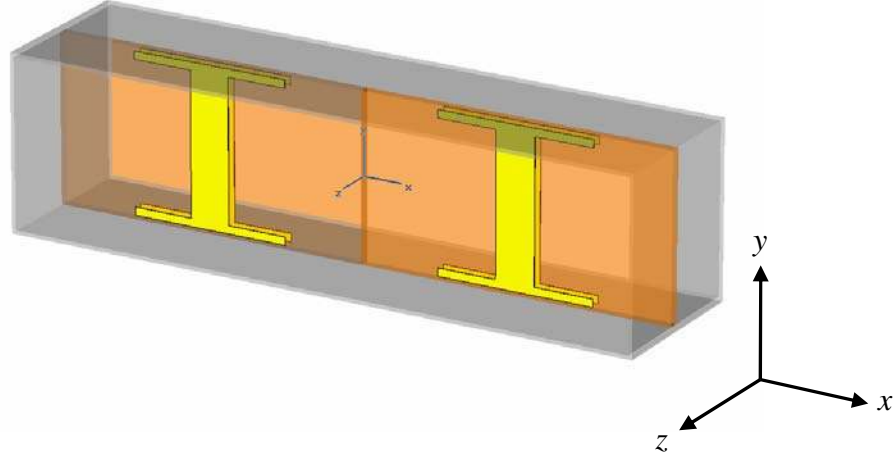
Figure 46.   Two Unit Cells of H Type Metamaterial with the Same Dimension Described in Model 4

The extracted permeability and permittivity are shown in Figures 47 and 48. Note that there is a second spike observed in both the real and imaginary parts of permittivity. This second peak only occurs in ε when the material is in the waveguide and arises from the $1/2a$ term in the numerator of Eq. (4.18). The peak disappears as $a \to \infty$ and normal incidence is simulated. As a practical matter, the material would not be used near resonance because the losses are high. Most published papers omit data near the resonant frequency, a range known to be hard to deal with in the retrieval of metamaterials parameters [24].

One possible source of this peak is that the extraction formulas assume an isotropic material. Formulas are available for extracting anisotropic materials in free space, but not for waveguide [23]. This feature needs further investigation.
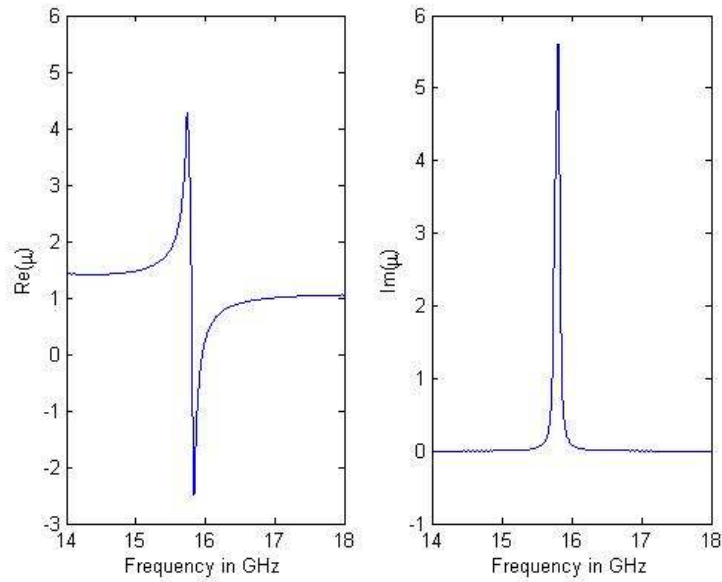
Figure 47.   Extracted Permeability of Model 6
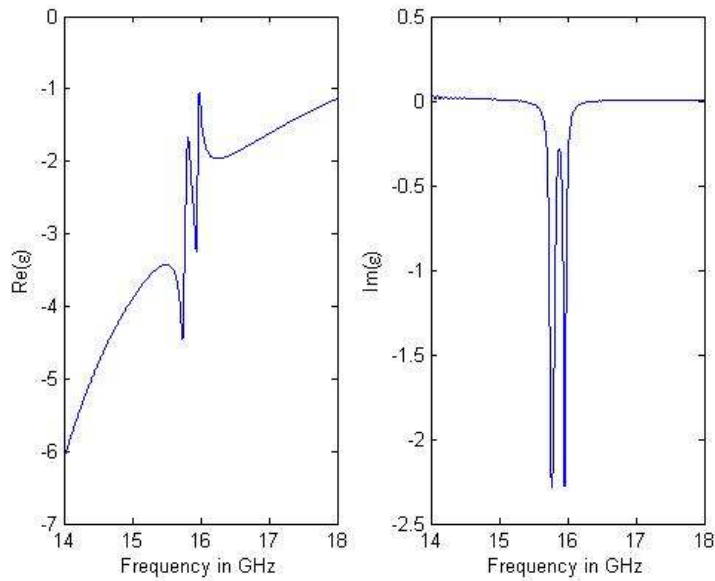
Figure 48.   Extracted Permittivity of Model 6

D.   SUMMARY

In this chapter, two models were used to extract the permeability and permittivity from the simulated S-parameters. The formulas used were based on samples in a waveguide environment, and therefore the image principle had to be applied in order to

treat the model as an infinite slab. Test cases were performed to verify the effectiveness of the simulation set up. It was found that the differences between the simulated and calculated S-parameter were negligible. Again, the resonant frequency of the metamaterial model was very sensitive to the mesh cell number; therefore, it is good to have both simulation and measurement data to compare. The models have shown that the waveguide environment program can work not only for normal materials but also metamaterials. In comparing model 4 with model 6, the extracted permeability and permittivity were very close. This result showed that both the free space and waveguide method can be used to retrieve the constitutive parameters of materials.

V.   CONCLUSION

A.   SUMMARY AND CONCLUSIONS

The basic concept of a metamaterial and the unusual properties of DNG materials were discussed. The applications of metamaterials in waveguide miniaturization, microwave devices and other possible applications were presented and explained. To employ metamaterials in devices it is necessary to know their effective permittivity and permeability. The information can be obtained by measurements on a sample in free space or waveguide. Alternately, simulation of the material in free space or a waveguide could be used.

The equations used in the free space environment to extract the constitutive parameters from simulated S-parameters were described and programmed in MATLAB. Test cases were used to validate the correctness of the simulation settings. Several different types of materials, including the normal (homogeneous) material and metamaterial were simulated in MWS and a retrieval program was used to extract the permittivity and permeability of the materials. The results were compared with published data. The resonant frequency of the results and its relationship to the dimensions of the inclusions and number of mesh cells at the simulation starting point was investigated and discussed.

The waveguide environment retrieval method and accompanying equations were discussed in Chapter IV. Boundary conditions were properly selected so that a small sample in the waveguide environment could be treated as an infinite panel. The same metamaterial (H-type inclusions) was examined using both the free space and waveguide methods to compare the extracted results.

It was shown that both the free space and waveguide methods could be used to successfully retrieve the constitutive parameters from the scattering parameters. In both free space and waveguide cases the number of mesh cells used at the simulation starting point, the dimensions of the inclusions, and the boundary condition settings in MWS were the key parameters for successful retrieval.

Finally, the simulation and extracted results of the effective parameters could be used as data for designing microwave devices with metamaterials. The simulation methods and extraction programs make the effective parameter determination much more efficient in time and cost than building large panels for testing.

B.   FUTURE WORK

In this thesis, normal and DNG materials were used to examine the retrieval programs. Single negative materials (SNG) were not included. Dealing with the SNG materials is more of a challenge because of the sign ambiguity in the square root of $\mu \cdot \varepsilon$ when it is programmed. More inputs must be acquired to decide the correct sign when using SNG materials. Future research could be conducted to validate the programs using thicker materials which are more realistic in terms of fabrication. In this research the sample thickness has been small compared to wavelength. This condition avoids many ambiguities that occur for thick samples. Future work could also be conducted to correct the errors due to the nonzero incidence so that the extracted results could be compared with the normal incident cases. Finally, the cause of the second resonance in ε that occurs in the waveguide needs to be examined further.

APPENDIX

A.   MATLAB CODE FOR FREE SPACE ENVIRONMENT

This appendix provides the MATLAB code used to retrieve the constitutive parameters from S-parameters in Chapter III. The code is written in MATLAB 7. This code retrieves and plots μ_r, ε_r, n, and Z as a function of frequency respectively.

```matlab
%#######################################################
% multiple frequency for plane wave incident on a panel
% sample has thickness d, free space case
%#######################################################
clear
clc
%***************************************************
% constants
rad=pi/180;
eps0=8.85e-12;
mu0=4*pi*1e-7;
eta0=sqrt(mu0/eps0);  % free space
c=1/sqrt(eps0*mu0);
%***************************************************
% variables
d=2.5e-3;   % thickness of the sample
f1=2e9; df=18e6; f2=20e9; Nf=floor((f2-f1)/df)+1; % frequency range and
spacing
%***************************************************
% load raw data
load M1r.m;
load M2r.m;
load P1r.m;
load P2r.m;
Mag1=M1r(:,2);
Mag2=M2r(:,2);
Ph1=-unwrap(P1r(:,2),180);
Ph2=-unwrap(P2r(:,2),180);
%*****************************************
% freqyency loop begin
for it=1:Nf
   f=f1+(it-1)*df;
   Fr(it)=f;
   Fghz(it)=f/1e9;
   fghz=f/1e9;
   Z0=eta0; W=2*pi*Fr(it); beta0=W/c;
   %*****************************************
   % combine magnitude and phase of the S11 and S21
    R(it)=Mag1(it)*exp(j*Ph1(it)*rad);
    T(it)=Mag2(it)*exp(j*Ph2(it)*rad);
   %*****************************************
```

```matlab
    % m loop begin
    Max=0; % ---------m value set up
    itt=0;
    for m=-Max:Max
    itt=itt+1;
    %**************************************************
    % using formulas from Robust method
    Tp=T(it);
    Z21(it)=sqrt(((1+R(it))^2-Tp^2)/((1-R(it))^2-Tp^2));
    Z22(it)=-sqrt(((1+R(it))^2-Tp^2)/((1-R(it))^2-Tp^2));
    expinkd1(it)=Tp/(1-R(it)*(Z21(it)-1)/(Z21(it)+1));
    expinkd2(it)=Tp/(1-R(it)*(Z22(it)-1)/(Z22(it)+1));
    if  abs(real(Z21(it)))>=0.005 & real(Z21(it))>=0
        expinkd(it)=expinkd1(it);
        Z2(it)=Z21(it);
    end
    if  abs(real(Z21(it)))>=0.005 & real(Z21(it))<0
        expinkd(it)=expinkd2(it);
        Z2(it)=Z22(it);
    end
    if abs(real(Z21(it)))<0.005 & abs(expinkd1(it))<=1
        expinkd(it)=expinkd1(it);
        Z2(it)=Z21(it);
    end
    if abs(real(Z21(it)))<0.005 & abs(expinkd1(it))>1
        expinkd(it)=expinkd2(it);
        Z2(it)=Z22(it);
    end
    ni(it)=-1/(beta0*d)*j*real(log(expinkd(it)));  % imag of n
    nr(it,itt)=1/(beta0*d)*(imag(log(expinkd(it)))+2*m*pi);  %real of n
    n2(it,itt)=nr(it,itt)+ni(it);
    Er2(it,itt)=n2(it,itt)/Z2(it);
    Mr2(it,itt)=n2(it,itt)*Z2(it);
    end  % end of m loop
end % end of frequency loop

figure(1)
subplot(121);
plot(Fghz,real(Mr2));
xlabel('Frequency in GHz')
ylabel('Re(\mu)')
subplot(122)
plot(Fghz,imag(Mr2));
xlabel('Frequency in GHz')
ylabel('Im(\mu)')

figure(2)
subplot(121);
plot(Fghz,real(Er2));
xlabel('Frequency in GHz')
ylabel('Re(\epsilon)')
subplot(122)
plot(Fghz,imag(Er2));
xlabel('Frequency in GHz')
ylabel('Im(\epsilon)')
```

```matlab
figure(3)
subplot(121);
plot(Fghz,real(n2));
xlabel('Frequency in GHz')
ylabel('Re(n)')
subplot(122)
plot(Fghz,imag(n2));
xlabel('Frequency in GHz')
ylabel('Im(n)')

figure(4)
subplot(121);
plot(Fghz,real(Z2));
xlabel('Frequency in GHz')
ylabel('Re(Z)')
subplot(122)
plot(Fghz,imag(Z2));
xlabel('Frequency in GHz')
ylabel('Im(Z)')
```

B. MATLAB CODE FOR WAVEGUIDE ENVIRONMENT

This appendix provides the MATLAB code used to retrieve the constitutive parameters from S-parameters in Chapter IV. The code is written in MATLAB 7. This code retrieves and plots μ_r, ε_r, n, and Z as a function of frequency respectively.

```matlab
%############################################################
% multiple frequency in a waveguide environment
% sample has thickness delta, total length of the waveguide is d1+delta+d2
%############################################################
clear
clc
a=16e-3;
delta=2.274e-3;
d1=1e-3;
d2=1e-3;
eps0=8.85e-12;
mu0=4*pi*1e-7;
c=1/sqrt(eps0*mu0);
rad=pi/180;
Z0=377;
%*************************************************
load M1r.m;
load M2r.m;
load P1r.m;
load P2r.m;
Mag1=M1r(:,2);
Mag2=M2r(:,2);
Ph1=-unwrap(P1r(:,2),180);
Ph2=-unwrap(P2r(:,2),180);
%*************************************************
it=0;
f1=14e9; df=4e6; f2=18e9; Nf=floor((f2-f1)/df)+1;
for it=1:Nf
    f=f1+(it-1)*df;  % must higher than the cut-off frequency in free space
    Fr(it)=f;
    w=2*pi*Fr(it); wave=c/f;
    Rm(it)=Mag1(it)*exp(j*Ph1(it)*rad);
    Tm(it)=Mag2(it)*exp(j*Ph2(it)*rad);
    beta0(it)=sqrt((w/c)^2-(pi/a)^2);
end
%*********************************************************
% make use of equation from Thomas
nfreq=it;
for it=1:nfreq
    Tt(it)=Tm(it)*exp(-j*beta0(it)*(d1+d2)); %---T
    Rr(it)=Rm(it)*exp(-j*2*beta0(it)*d1);  %---R
    %*****************************************************
    % to get Z2
    b=(Rr(it)^2-Tt(it)^2+1)/(2*Rr(it));
    R21=b+(sqrt(b^2-1));
    R22=b-(sqrt(b^2-1));
```

```matlab
    Rn=nan;
    if abs(R21)<=1
        RR=R21; Rn=RR; %---R2
    end
    if abs(R22)<=1
        RR=R22; Rn=RR;
    end
    if (abs(R21)<1 & abs(R22)<1) | (abs(R21)==1 & abs(R22)==1)
        disp(['both solutions give |R|<1 for fghz = ',num2str(fghz)])
    end
    Z=(1+RR)/(1-RR);
    sgn=1; if real(Z)<0, sgn=-1; end
    Z2(it)=Z*sgn;
    %----------------------------------------------------------------
    k=0;  % need to be determined
    %----------------------------------------------------------------
    K=Rr(it)^2-Tt(it)^2+1;
    r1=(K+sqrt(K^2-4*Rr(it)^2))/2/Rr(it);
    r2=(K-sqrt(K^2-4*Rr(it)^2))/2/Rr(it);
    if abs(r1)<=1
        r=r1;
    end
    if abs(r2)<=1
        r=r2;
    end
    t=(Rr(it)+Tt(it)-r)/(1-r*(Rr(it)+Tt(it)));
    gamma=(j*2*k*pi-log(t))/delta;
    gamma0=-j*2*pi*sqrt(Fr(it)^2*mu0*eps0-(1/2/a)^2);
    Mr(it)=mu0*(gamma*(1+r)/gamma0/(1-r));
    Er(it)=(((1/2/a)^2-(gamma/2/pi)^2)/Mr(it)/Fr(it)^2);
    Mre(it)=Mr(it)/mu0;
    Ere(it)=Er(it)/eps0;
    n2(it)=Mre(it)/Z2(it);
end   % end of frequency loop

figure(1)
subplot(121);
plot(Fr/1e9,real(Mre));
xlabel('Frequency in GHz')
ylabel('Re(\mu)')
subplot(122)
plot(Fr/1e9,imag(Mre));
xlabel('Frequency in GHz')
ylabel('Im(\mu)')

figure(2)
subplot(121);
plot(Fr/1e9,real(Ere));
xlabel('Frequency in GHz')
ylabel('Re(\epsilon)')
subplot(122)
plot(Fr/1e9,imag(Ere));
xlabel('Frequency in GHz')
ylabel('Im(\epsilon)')
```

```
figure(3)
subplot(121);
plot(Fr/1e9,real(n2));
xlabel('Frequency in GHz')
ylabel('Re(n)')
subplot(122)
plot(Fr/1e9,imag(n2));
xlabel('Frequency in GHz')
ylabel('Im(n)')

figure(4)
subplot(121);
plot(Fr/1e9,real(Z2));
xlabel('Frequency in GHz')
ylabel('Re(Z)')
subplot(122)
plot(Fr/1e9,imag(Z2));
xlabel('Frequency in GHz')
ylabel('Im(Z)')
```

LIST OF REFERENCES

1. Hannan, P. W. & Balfour, M. A., "Simulation of a Phased-Array Antenna in Waveguide," *IEEE Trans. on Antennas and Propagation.* Vol. 13, Issue 3, May 1965 Page(s):342 - 353.

2. McGinnis, Dave, "Electromagnetic Properties of ECCOSORB MF-190," Pbar Note 566 (www-bdnew.fnal.gov/pbar), May 1997.

3. Sun, Ding, "Measurement of Complex Permittivity and Permeability of Microwave Absorber ECCOSORB MF-190," Pbar Note 576 (www-bdnew.fnal.gov/pbar), August 1997.

4. McGinnis, Dave, "Measurement of Relative Permittivity and Permeability Using Two Port S-parameter Technique," Pbar Note 585 (www-bdnew.fnal.gov/pbar), April 1998.

5. Zwick, Thomas, Chandrasekhar, Arun, Baks, Christian W., Pfeiffer, Ullrich R., Brebels, Steven, & Gaucher, Brian P., "Determination of the Complex Permittivity of Packaging Materials at Millimeter-Wave Frequencies," *IEEE Trans. Microwave Theory Tech.* **54**, No. 3, (2006).

6. Jenn, D., Notes for EC3630 (Radiowave Propagation), Naval Postgraduate School, 2003 (unpublished).

7. Veselago, V. G., "The Electrodynamics of Substances with Simultaneously Negative Values of μ and ε," *Sov. Phys. Usp.*, **10**, 509, (1968).

8. Pendry, J. B., Holden, A. J., Stewart, W. J., & Young, I., "Extremely Low Frequency Plasmons in Metallic Mesostructures," *Phys. Rev. Lett.*, **76**, 4773, (1996).

9. Pendry, J. B., Holden, A. J., Robbins, D. J., & Stewart, W. J., "Magnetism from conductors and enhanced nonlinear phenomena," *IEEE Trans. Microwave Theory Tech.,* **47**, 2075, (1999).

10. Pendry, J. B., "Negative Refraction Makes a Perfect Lens," *Phys. Rev. Lett.,* **85**, 3966, (2000).

11. Smith, D. R., Padilla, Willie J., Vier, D. C., Nemat-Nasser, S. C., & Schultz, S., "Composite Medium with Simultaneously Negative Permeability and Permittivity," *Phys. Rev. Lett.*, **84**, 4184, (2000).

12. Shelby, R. A., Smith, D. R., & Schultz, S., "Experimental Verification of a Negative Index of Refraction," *Science*, **292**, 77, (2001).

13. Ziolkowski, R. W. & Engheta, N., "A positive future for double-negative metamaterials," *IEEE Trans. Microwave Theory Tech.*, **53**, No. 4, (2005).

14. Smith, D. R., Pendry, J. B., & Wiltshire, M. C. K., "Metamaterials and Negative Refractive Index," *Science,* Vol. 305 (2004).

15. Hrabar, Silvio, Bartolic, Juraj, & Sipus, Zvonimir, "Waveguide Miniaturization Using Uniaxial Negative Permeability Metamaterial," *IEEE Trans. on Antennas and Propagation.,* **53**, No. 1, (2005).

16. Jakšic´, Zoran, Dalarsson, Nils, & Maksimovic´, Milan, "Negative Refractive Index Metamaterials: Principles and Applications," *Microwave Review*, Jun. 2006.

17. Elefttheriades, G. V., "Negative-Refractive-Index Transmission-Line Metamaterials and Enabling Microwave Devices," *The Radio Science Bulletin*, No. 312 (2005).

18. Cotuk, Unit, "Scattering from Multi-layered Metamaterials Using Wave Matrices," Naval Postgraduate School Thesis, Sept. 2005.

19. Chen, Xudong, Grzegorczyk, Tomasz M., Wu, Bae-Ian, Pacheco Jr., Joe, & Kong, Jin Au, "Robust Method to Retrieve the Constitutive Effective Parameters of Metamaterials," *Phys. Rev. E.,* **70**, 016608, (2004).

20. Smith, D. R., Vier, D. C., Koschny, Thomas, & Soukoulis, C. M., "Electromagnetic Parameter Retrieval from inhomogeneous metamaterials," *Phys. Rev. E.,* **71**, 036617, (2005).

21. Zhou, Jiangfeng, Zang, Lei, Tuttle, Gary, Koschny, Thomas, & Soukoulis, Costas M., "Negative index materials using simple short wire pairs," *Phys. Rev. B.*, **73**, 041101, (2006).

22. Zhou, Jiangfeng, Koschny, Thomas, Zhang, Lei, Tuttle, Gary, & Soukoulis, Costas M., "Experimental demonstration of negative index of refraction," *Applied Phys. Lett.*, **88**, 221103, (2006).

23. Zwick, Thomas, Chandrasekhar, Arun, Baks, Christian W., Pfeiffer, Ullrich R., Brebels, Steven, & Gaucher, Brian P., "Determination of the Complex Permittivity of Packaging Materials at Millimeter-Wave Frequencies," *IEEE Trans. Microwave Theory Tech.*, **54**, No. 3, (2006).

24. Chen, Xudong, Wu, Bae-Ian, Kong, Jin Au, & Grzegorczyk, Tomasz M., "Retrieval of the Effective Constitutive Parameters of Bianisotropic Metamaterials," *Phys. Rev. E.,* **71**, 046610, (2005).

INITIAL DISTRIBUTION LIST

1.   Defense Technical Information Center
   Ft. Belvoir, Virginia

2.   Dudley Knox Library
   Naval Postgraduate School
   Monterey, California

3.   Chairman
   Information Sciences Department
   Monterey, California

4.   Professor David C. Jenn
   Department of Electrical and Computer Engineering
   Monterey, California

5.   Professor Michael A. Morgan
   Department of Electrical and Computer Engineering
   Monterey, California

6.   C.S.I.S.T. Library
   Taoyuan, Taiwan R.O.C.